Precipitation in the mountains of Central Asia: isotopic composition and source regions

Zarina Saidaliyeva[1], Maria Shahgedanova[1], Vadim Yapiyev[1,2], Andrew John Wade[1], Fakhriddin Akbarov[3], Mukhammed Esenaman uulu[4], Olga Kalashnikova[4], Vassiliy Kapitsa[5], Nikolay Kasatkin [5], Ilkhomiddin Rakhimov[6], Rysbek Satylkanov[7], Daniiar Sayakbaev[7], Eleonora Semakova[8], Igor Severskiy[5], Maxim Petrov[3], Gulomjon Umirzakov[9], and Ryskul Usubaliev[4]

[1]Department of Geography and Environmental Science, University of Reading, Reading, RG66AB, UK;
[2]School of Mining and Geosciences, Nazarbayev University, Astana, 010000, Kazakhstan
[3]Institute of Geology and Geophysics, Tashkent, 100164, Uzbekistan;
[4]Central-Asian Institute for Applied Geosciences, Bishkek, 720027, Kyrgyzstan;
[5]Central Asian Regional Glaciological Centre Under the Auspices of UNESCO, Almaty, 050010, Kazakhstan;
[6]Institute of Water Problems, Hydropower and Environment, Dushanbe, 734025, Tajikistan;
[7]Tien-Shan High Mountain Scientific Centre, Bishkek, 720033, Kyrgyzstan;
[8]Ulugh Beg Astronomical Institute of the Uzbekistan Academy of Science Tashkent, 100052, Uzbekistan;
[9]National University of Uzbekistan, Tashkent, 100174, Uzbekistan;

Correspondence to: Zarina Saidaliyeva (z.saidaliyeva@pgr.reading.ac.uk)

Abstract. Isotopic composition of precipitation in the mountains of four Central Asian countries (Kazakhstan, Kyrgyzstan, Tajikistan and Uzbekistan) was measured using 908 event-based precipitation samples collected at eight sites in 2019 – 2021, and 7 monthly samples from Dushanbe (Tajikistan) thereby filling a gap in stable isotope data for the region. Regional and seasonal patterns of δ^{18}O, δD and D-excess were investigated. Local Meteoric Water Lines (LMWL) derived using seven regression methods using both non-weighted and weighted precipitation. It is recommended that the non-weighted Ordinary Least Squares Regression (OLSR) and Reduced Major Axis Regression (RMA) methods can be applied across the region except in summer, when the Precipitation-Weighted Least Squares Regression (PWLSR) method is recommended. An atmospheric back trajectory analysis and a mixing model were applied in combination for the first time, using the δ^{18}O, δD and D-excess data, to identify the atmospheric moisture source regions and quantify the relative importance. The main distant sources were the Black and Caspian Seas region, Iran – eastern Mediterranean, and northern Kazakhstan – Siberia. The recycled moisture from the irrigated lower reaches of the Amu Darya and Syr Darya rivers, and from the study catchments, accounted for 29–71% of the atmospheric moisture reaching the observation points. In spring, summer and winter, in the Chon-Kyzyl-Suu catchment, up to 85% of the precipitation was estimated to be derived from local re-evaporation, most likely from Lake Issyk Kul. These findings highlight the importance of moisture from terrestrial sources, especially irrigated land, in precipitation formation in Central Asia.

1 Introduction

Atmospheric precipitation is the primary source of water which contributes to river runoff in the mountains of Central Asia (CA) directly and by sustaining seasonal snowpack and glaciers, whose meltwater maintains river flow in the dry season. In CA, precipitation is characterised by strong spatial variability due to large changes in elevation (from about 700 m above sea level (a.s.l.) up to 7000 m a.s.l.) over relatively short distances and the mountain ridge and valley positions in relation to the moisture-bearing flow (Lydolph, 1977; Aizen et al., 1997). Longer-term changes and interannual variability in precipitation affect all components of CA water resources (Shahgedanova, 2002; Jin et al., 2012; Aizen et al., 2017) and there is strong evidence for a decline in glacier area and negative glacier mass balance (Kutuzov and Shahgedanova, 2009; Farinotti et al., 2015; Severskiy et al., 2016; Kapitsa et al., 2020), attributed not only to the observed increase in temperature, but also to prolonged negative precipitation anomalies observed in the 1970s-1980s (Shahgedanova et al., 2018; Hoelzle et al., 2019). Future projections of precipitation in CA are characterised by strong uncertainty. Although overall, the Coupled Model

Intercomparison Project Phase 6 (CMIP6) projects an increase in annual precipitation in high mountains in the future, the projected changes vary between regions and seasons especially over the plains and foothills, and uncertainty remains about

45 how these changes will be offset or enhanced by changes in evaporation and atmospheric circulation (Jiang et al., 2020). This leads to a cascade of uncertainties in impact assessments using glacier mass balance, hydrological, water resource, and crop models. A better understanding of sources of precipitation and moisture cycling, links between changes in atmospheric circulation and precipitation, and its responses to climatic warming is essential for water management and food production in the water-deficient regions of CA (Kaser et al., 2010; Immerzeel et al., 2020; Viviroli et al., 2020).

50 Analysis of the isotopic composition of precipitation can be used to constrain some of these uncertainties (Yoshimura, 2015; Putman et al., 2019; Jasechko, 2019). Stable isotopes of hydrogen and oxygen are useful indicators of the meteorological history of atmospheric water from evaporation, through transportation and condensation, to precipitation because these processes control fractionation which, in turn, controls isotopic composition. The ratios of heavy (^{18}O) to light (^{16}O) isotopes of oxygen (δ^{18}O) and deuterium (D) to light hydrogen (^{1}H) (δD) and the relationship between δD and δ^{18}O, known as Global

55 Meteoric Water Line (GMWL) and approximated by Equation (1), have been widely applied in hydrometeorology since the 1960s (Craig, 1961; Craig and Gordon, 1965):

$$\delta D = 8 \times \delta^{18}O + 10 \tag{1}$$

Rozanski et al. (1993) investigated δD and oxygen δ^{18}O relationships using the data from the Global Network of Isotopes in Precipitation (GNIP) sites and suggested that Local Meteoric Water Lines (LMWL) provide a better representation of isotopic

60 composition of regional precipitation because they depend on latitude, continentality, altitude, and regional climatic anomalies. The relation of GMWL to LMWL helps to identify regional characteristics and processes affecting precipitation (Wang et al., 2018; Putman et al., 2019). It is used together with the concept of deuterium excess (D-excess; Equation 2) proposed by Dansgaard (1964) to characterise sources of moisture where:

$$\text{D-excess} = \delta D - (8 \times \delta^{18}O) \tag{2}$$

65 The global average D-excess is 10‰. In general, moisture recycling increases and sub-cloud evaporation reduces D-excess. Increased D-excess in precipitation results from the significant addition of re-evaporated moisture from continental basins, while lower values characterise moisture originating from the oceans. This enables distinction to be made between moisture from distant ocean and local sources in continental interiors (Araguás-Araguás et al., 2000; Pang et al., 2011; Aemisegger et al., 2014; Bershaw, 2018) particularly when D-excess is used in conjunction with atmospheric back-trajectory analysis (Wang

70 et al., 2017, 2019; Bershaw, 2018). Although non-equilibrium fractionation and evaporation are two major processes controlling D-excess, sub-cloud evaporation in a warm and dry air column changes D-excess further obscuring the original vapor composition (Friedman et al., 1962), and D-excess in the cloud condensate may be substantially different from D-excess in precipitation samples collected at ground level (Froehlich et al., 2008). The sub-cloud evaporation effect is significant in arid regions where precipitation intensity is low (Juhlke et al., 2019). Isotopic composition and D-excess can also change with

75 altitude (Bershaw, 2018; Natali et al., 2022; Yang et al., 2023) due to sub-cloud evaporation, the variation in distance travelled by a raindrop, and the transition from upwind to the downwind rain shadow, whereby lower temperature and high humidity cause lower evaporation on the upwind slopes as orographic precipitation forms. Sub-cloud evaporation and a shorter distance travelled by a raindrop are known to increase D-excess values, while the rain shadow is known to reduce them, thereby making D-excess a useful proxy not only for precipitation sources but also for changes in airmass moisture over its pathway.

80 While the use of isotopic analysis in hydrometeorology increases globally (Yoshimura, 2015; Aggarwal et al., 2016; Jasechko, 2019), knowledge about the isotopic composition of precipitation in CA (defined here as Kazakhstan (KZ), Kyrgyzstan (KG), Tajikistan (TJ), Turkmenistan, and Uzbekistan (UZ)) is limited. Currently, the Global Network of Isotopes in Precipitation

(GNIP) database contains only seven measurements of δD and δ¹⁸O from the precipitation samples collected in Tashkent, Uzbekistan (IAEA/WMO, 2015). This contrasts to extensive measurements in the Chinese Tien Shan (Pang et al., 2011; Wang

85   et al., 2016b, 2018; Chen et al., 2021) where the Chinese Network of Isotopes in Precipitation (CHNIP) became operational in 2004 (Liu et al., 2014; Zhang and Wang, 2018).

The lack of CA precipitation isotope data constrains the LMWL development and understanding and quantifying regional contributions to precipitation. In contrast to the Chinese Tien Shan where the events-based precipitation samples were analysed (Pang et al., 2011; Wang et al., 2016b, 2018; Chen et al., 2021), in CA, ice-core isotopic compositions in the central Tien Shan

90   (Inylchek Glacier; 42º09'N; 79º56'E , 5200 m a.s.l.) and Pamir (Fedchenko glacier; 38º15'N; 72º15'E, at two sampling sites with elevation 5206 and 5365 m a.s.l.) were used to characterise moisture sources and changes in regional atmospheric circulation patterns (Aizen et al., 1996, 2004, 2009; Kreutz et al., 2003). Moisture sources for the Inylchek glacier were established broadly as the Atlantic Ocean, Mediterranean and Black Seas on the basis of δ¹⁸O analysis combined with the catalogue of weather types (Aizen et al., 2004). Most precipitation over the Pamir originated in the Atlantic according to Aizen

95   et al. (2009). The dominant source of moisture for the western Pamir were identified as the Mediterranean and Caspian Seas which was confirmed by high D-excess values of 20‰ measured in snow and ice cores by Bershaw (2018). However, in the western Pamir, according to the event-based precipitation samples and trajectories analysis, D-excess was lower at 13‰ leading to the conclusion that the Mediterranean contributed about 20% of the total moisture (Juhlke et al., 2019). This discrepancy may be due to the uncertainty in linking ice core samples to moisture trajectories, or because regional source

100   signals are altered in CA along the long moisture transportation routes (Bershaw, 2018). Insufficient data on precipitation isotopic composition mean current inferences are uncertain.

To fill the data and knowledge gaps, a sampling campaign was conducted between 2019 and 2021 by the Central Asia Research and Adaptation Water Network (CARAWAN) in five catchments located predominantly in the mountains. Over 900 event-based precipitation samples were collected and processed, generating an extensive database of δD, δ¹⁸O, and D-excess values.

105   The overall aim of the presented work is to determine the mountain precipitation source areas and to help achieve this, four objectives are defined to: (i) evaluate precipitation stable-isotope spatial and temporal variations in the mountains of CA; (ii) characterise isotope dependency on geographical location, temperature, and amount of precipitation; (iii) develop LMWL to aid future assessment of the relative contributions of different of water sources to streamflow, groundwater recharge, and isotope mass balance studies; and (iv) establish a relationship between variations in isotopic composition of precipitation and

110   its source regions.

2 Data and methods

2.1 Sampling points and characteristics of study area

The eight sampling sites were located in the Tien Shan and Pamir-Alai mountains and their foothills (Fig. 1a) between 1255 and 3277 m a.s.l., with two sites located in the foothills at lower elevations (Table 1). The regional climate is continental arid

115   in the south and semi-arid in the north (Lydolph, 1977; Shahgedanova, 2002) with strong seasonality and altitudinal change in temperature and precipitation (Fig 1 b, c). Annual precipitation ranges between 100 mm a⁻¹ in the deserts of Uzbekistan and southern-western Kazakhstan to 1200 a⁻¹ mm in the mountains. The locations of the major mountain ranges is an important control over precipitation and while the outer ranges receive ample precipitation during the wet season, intermontane basins are arid (Lydolph, 1977; Aizen et al., 1997). In the southern part of the region, summer temperatures are high and precipitation

120   is extremely low (Fig. 1 b, c). Precipitation starts increasing in October when regional atmospheric circulation is dominated by the westerly flow and, across most of the region, precipitation peaks in spring occurring earlier (March-April) in the south

and later (April-May) in the north. At higher elevations in the northern Tien Shan, the precipitation maximum is between May and July (Fig. 1c). In winter, the northern part of the region is dominated by the Siberian anticyclone and precipitation is low.
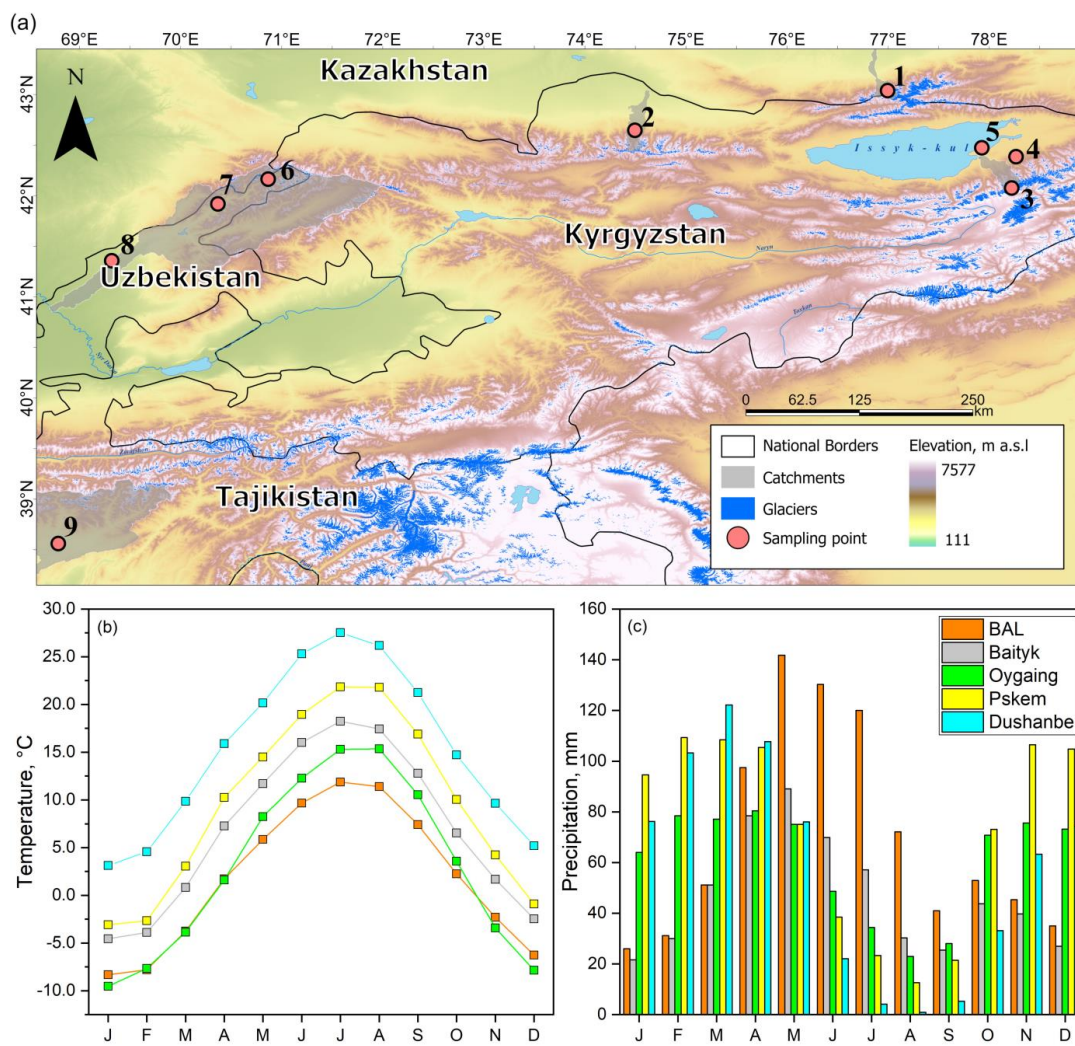
125

Figure 1: (a) Study area and locations of the sampling sites: (1) Bolshoe Almatinskoe Lake (BAL), (2) Baityk, (3) Karabatkak Glacier, (4) Lesnoy Cordon, (5) Tien-Shan High Mountain Scientific Centre (TSC), (6) Oygaing (meteorological station Maydantal), (7) Pskem, (8) Tashkent, and (9) Dushanbe. Digital Elevation Model (DEM) derived from the Shuttle Radar Topography Mission (SRTM) is used as background (available from https://lpdaac.usgs.gov/about/citing_lp_daac_and_data).

130 Glacier outlines are from the Global Land Ice Measurements from Space (GLIMS) database (Consortium, 2017). National borders and water bodies are from ESRI ArcGIS Hub. (b) Mean monthly temperature and (c) mean monthly precipitation in the 1980-2015 period. Sampling sites are numbered as in Table 1.

2.2 Event-based sampling of precipitation and design of laboratory isotopic analysis

The event-based precipitation samples and meteorological data (daily air temperature, amount and type of precipitation) were
135   collected between 2019 and 2021 in five mountainous catchments at eight sampling sites generating, in total, 908 precipitation
samples (Fig. 1a; Table 1). Seven samples of monthly precipitation were collected in Dushanbe using a PALMEX rain sampler
(http://www.rainsampler.com/portfolio-page/rain-sampler-rs1/).

Table 1: Characteristics of sampling sites (Fig. 1a) and details of the sampling programme. N is number of samples.

Site number	Sampling sites	Catchment	Country	Lat (N)	Lon (E)	Elevation (m a.s.l)	Period	N	N with precipitation depth data
1	Bolshoe Almatinskoe Lake (BAL)	Ulken Almaty (UA)	KZ	43.04	76.99	2563	May 2019 - October 2021	338	332
2	Baityk	Ala-Archa (AA)	KG	42.65	74.50	1588	July 2019 - May 2021	115	115
3	Karabatkak Glacier		KG	42.16	78.27	3277	August 2019 - August 2021	37	35
4	Lesnoy Cordon	Chon Kyzyl-Suu (CKS)	KG	42.19	78.20	2571	May 2019 - August 2021	117	114
5	Tien-Shan High Mountain Scientific Centre (TSC)		KG	42.35	78.02	1775	February 2020 - July 2021	29	-
6	Oygaing		UZ	42.00	70.64	1490	Junuary 2020 - October 2021	196	196
7	Pskem	Chirchik (CHK)	UZ	41.92	70.37	1255	November 2020 - July 2021	30	30
8	Tashkent		UZ	41.36	69.32	486	November 2020 - October 2021	46	46
9	Dushanbe*	Kofarnihon (K)	TJ	38.56	68.79	816	October 2018 - October 2019	7	6
			Total					915	874

140   *Cumulative monthly precipitation

Rainfall samples were collected immediately after the precipitation events and precipitation depth was measured. The samples
were filtered using the 0.2 μm filters at the sampling sites and stored in 2 ml glass vials with screw caps pre-washed several
times with the filtered rainwater. Snowfall samples were melted at room temperature, filtered (0.2 μm), and placed in the 2 ml
145   glass vials. To avoid evaporation, all vials were sealed with Parafilm M (Bemis Company, USA, Part no. PM-992) and stored
at 4ºC.

The samples were analysed using a Picarro Isotopic Water Analyzer (L2120-I) with measurement precision of ±0.6‰ and
±0.2‰ for δD and δ^{18}O, respectively. The sample analysis procedures and quality were assessed and certified by the
International Atomic Energy Agency (IAEA) through the completion of a round-robin test using samples supplied by IAEA
150   and according to the procedure and criteria outlined in Wassenaar et al. (2021).

The samples were injected into the analyzer seven times sequentially, and the first three measurements were discarded to avoid
any memory effect from the previous samples. The remaining four measurements were checked for consistency using the
criterion of standard deviation not exceeding 1.5‰ and 0.15‰ for δD and δ^{18}O, respectively. The final values were calculated
as means of the four valid measurements. If four measurements, satisfying these conditions could not be obtained, the samples

155 were re-measured and average of at least three valid measurements was recorded (52 samples). The isotopic ratios were
recorded using delta-notation in *per mille* (‰) relative to the Vienna Standard Mean Ocean Water (V-SMOW):

$$\delta = (\frac{R_{sample}}{R_{standard}} - 1) \times 1000‰ \qquad (3)$$

where R_{sample} and $R_{standard}$ are the isotope ratios $^2H/^1H$ or $^{18}O/^{16}O$ of the samples and the standard, respectively. Two primary
(SMOW and Standard Light Antarctic Precipitation (SLAP)) and two secondary standards were used. The secondary standards

160 were: Tuyuksu Snow Melt Water (TSMW) collected from the Tuyuksu glacier in the study area with δD of –122.0‰ and $\delta^{18}O$
of –17.2‰, and commercially available Spring Water (SW) with δD of –55.0‰ and $\delta^{18}O$ of –8.5‰.

2.3 Local Meteoric Water Line (LMWL)

There are two approaches to defining LMWL. The first one gives equal weighting to all data points regardless of the amount
of precipitation they represent. This approach potentially increases uncertainty in the interpretation of results because samples

165 from smaller precipitation events tend to have lower D-excess due to the sub-cloud evaporation leading to sample enrichment
while samples from heavy precipitation events tend to be more depleted (Hughes and Crawford, 2012; Crawford et al., 2014).
To overcome this problem, weighted precipitation is used. This method requires data on precipitation depth which were
available in this study (Table 1). Both approaches were used for comparison and to produce recommendations on LMWL
development in the study region.

170 Ordinary Least Squares Regression (OLSR) was used to define LMWL with unweighted samples (n=915; Table 1).
Precipitation amounts were recorded for 874 samples (Table 1) which were used in the precipitation-weighted analysis. Six
regression methods were applied to the event-based precipitation samples: three non-weighted (OLSR, Reduced Major Axis
Regression (RMA), and major axis regression (MA)) and three precipitation-weighted (Precipitation-Weighted Least Squares
Regression (PWLSR), Precipitation-Weighted Reduced Major Axis Regression (PWRMA), and Precipitation-Weighted Major

175 Axis Regression (PWMA)) (Hughes and Crawford, 2012; Crawford et al., 2014). The Local Meteoric Water Line Freeware
(available at http://openscience.ansto.gov.au/collection/879) was used in all calculations. The software calculates the following
parameters: slope of regression line (a), standard deviation of the slope (sa), intercept of regression line (b), standard deviation
of the intercept (sb), average value of the sum of the squared errors of three methods OLSR, RMA and MA (or three
precipitation weighted) regressions, root mean Sum of Squared Errors (RMSSE), which allow inter-comparison of the different

180 regression methods. The proximity of the RMSSE values to 1.0 was used as an indicator of the method suitability for the
analysed data set. The t-test was applied to evaluate statistical significance of a difference between OLSR and each other
regression method.

2.4 Back trajectory modelling and cluster analysis using HYSPLIT

Isotopic composition of precipitation is determined by the combination of the origin of moisture and history of atmospheric

185 water transport and local conditions (Rozanski et al., 2013). To evaluate the controls of atmospheric circulation over the
isotopic composition of precipitation and characterise its sources, $\delta^{18}O$, δD, and D-excess values were used in the atmospheric
back trajectory analysis using the HYbrid Single-Particle Lagrangian Integrated Trajectory (HYSPLIT) model (version 5.2.0)
run with the Global Data Assimilation System (GDAS) meteorological input (Draxler and Rolph, 2013; Stein et al., 2015;
Rolph et al., 2017). HYSPLIT has horizontal resolution of 1º. For each precipitation event sampled at BAL (UA), Lesnoy

190 Cordon (CKS), Baityk (AA), and Oygaing (CHK) (Table 1), three-dimensional back trajectories were calculated using the site
locations and elevations as starting points. The starting time of each back trajectory was defined as the closest hour of the
precipitation event start, and the length of integration was 120 hours because uncertainty in the calculation of trajectories
increases with time afterwards (Draxler and Rolph, 2013). In line with previous studies (Jorba et al., 2004; Wu et al., 2015;

Pérez et al., 2015; Bagheri et al., 2019) and to comply with the HYSPLIT cluster analysis function requirements, single
195   trajectories were calculated instead of trajectory ensembles, potentially introducing uncertainty.

The generated back trajectories were grouped using cluster analysis based on minimizing distance and maximizing difference
between clusters with distinct trajectories (Dorling et al., 1992) and performed using the HYSPLIT 5.2.0 built-in cluster
analysis function (available at https://www.ready.noaa.gov/HYSPLIT_hytrial.php) for the selected four sampling sites.
Trajectories calculated for all events observed at each site throughout the year were grouped. Isotopic ratios and D-excess
200   values were initially analysed for the clusters generated for each site and season. However, many trajectory clusters generated
for different sites were similar (e.g., westerly trajectory cluster was generated for each site; see Fig. 7 further in the text).
Splitting the data by season for each site resulted in a small number of members in each cluster. To overcome this problem,
similar trajectory clusters from different sites were merged to form 'synoptic circulation groups'. Some of the groups included
data from all sites (e.g. westerly) while others were limited to a smaller number of sites. Analysis of the isotopic ratios and D-
205   excess was then performed by the 'synoptic circulation groups' and meteorological seasons. Analysis of variance (ANOVA)
and pairwise t-tests were used to test whether the differences between δ^{18}O, δD, and D-excess values attributed to different
groups were significant at a 95% confidence level.

2.5 Quantifying relative contributions of the identified moisture sources to total precipitation.

Source regions of moisture and its transport pathways were characterised using the cluster analysis of the HYSPLIT back
210   trajectories. The proportional contributions of multiple sources to total precipitation were quantified using a linear mixing
model whereby two isotopic signatures (δ^{18}O and δD) enable partitioning of the total precipitation between three sources
(Phillips and Gregg, 2001). The isotopic signatures of precipitation samples attributed to a source, identified via the cluster
analysis of back trajectories, were determined and mean signature values of δ^{18}O and δD were calculated for each source and
their mixture. Fractional contributions were calculated using Equations (4) and (5) (Phillips and Gregg, 2001):

215    $$\delta_P = f_A\delta_A + f_B\delta_B + f_C\delta_C \qquad (4)$$

$$f_A + f_B + f_C = 1 \qquad (5)$$

where f_A, f_B and f_C are fractional contributions of different moisture sources to local precipitation, $\delta_A, \delta_B, \delta_C$ are their isotopic
signature values, and δ_P is seasonal mean isotopic value for all precipitation events during the sampling period. The software
IsoError Version 1.04 (available at http://www.epa.gov/eco-research) (Phillips and Gregg, 2001)) was used to apply the mixing
220   model.

3 Results

3.1 Seasonal and spatial variability in δD and δ^{18}O.

The descriptive statistics of δD and δ^{18}O derived from all even-based precipitation events at each catchment are summarized
in Figure 2 and in Table S1 (where data are shown for each sampling site and for three types of precipitation: snow, rain and
225   mixed).

Rain samples (n=528) were characterized by higher mean δ^{18}O and δD values of –4.9‰, and −28.1‰, respectively whereas
snow samples (n=260) have lower mean δ^{18}O and δD values of −15.4‰ and −110.7‰, respectively (Table S1 and Fig. 4
further in the text). Variability in the snow data set was higher than in the rain data set with standard deviations of ±5.5‰
(δ^{18}O) and ±44.6‰ (δD) for snow and ±4.3 ‰ (δ^{18}O) and ±30.0‰ (δD) for rain. This is because in winter, day-to-day
230   temperature fluctuations, associated with changing synoptic conditions, are stronger than in summer with mean temperature
changes between two consecutive days of 4ºC (Shahgedanova, 2002). The mixed precipitation data set, based on 120 samples,

showed intermediate values of δ¹⁸O of −9.7‰ and δD of −61.7‰. Contrary to the expectation that standard deviations of the mixed precipitation isotopic ratios should be the highest, reflecting different proportions of solid and liquid content of precipitation in a sample, their values were the lowest for δ¹⁸O and broadly the same as for rain for δD (Table S1).

235

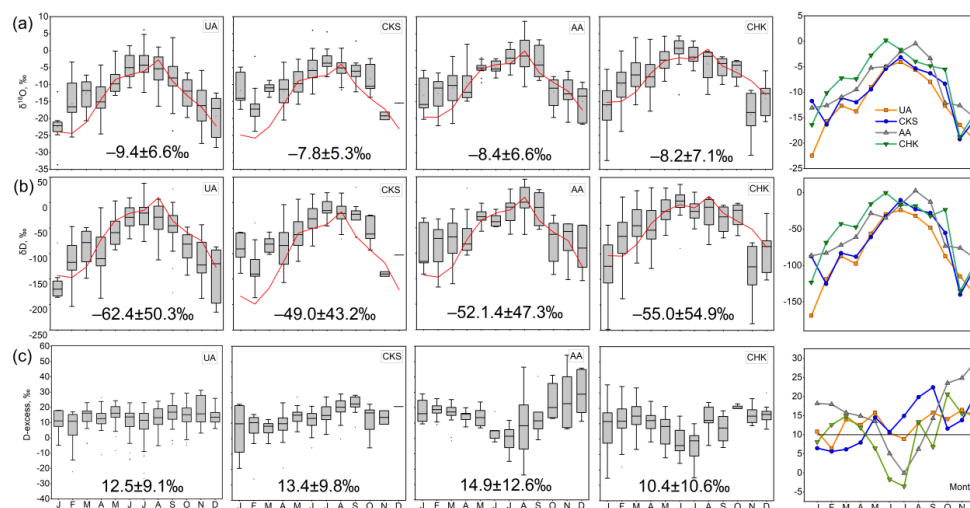Figure 2: Boxplots of (a) δ¹⁸O, (b) δD, and (c) D-excess in precipitation at four catchments (see Fig. 1 and Table 1 for locations and number of samples). Annual mean values ± standard deviation are shown. Straight line in (c) shows global mean D-excess value. The red line shows data from the Waterisotopes Database (Bowen, 2022). The Waterisotopes Database data were
240 averaged over all sampling location for catchments with more than one sampling site (CKS and CHK).

Clear seasonal cycles were observed in δD and δ¹⁸O values in each catchment where precipitation is enriched in heavy isotopes in summer and depleted in winter (Fig. 2a, b; Table S1). The stable isotope composition of event-based precipitation varied widely from −33.6 to 8.6‰ for δ¹⁸O and from −258.8 to 45.2‰ for δD, with overall means of −8.6 ± 6.5‰ and 56.2 ± 50.2‰,
245 respectively (Fig. 2a, b). Hydrogen is more susceptible to fractionation and less stable than oxygen and, therefore, δD exhibits greater variability than δ¹⁸O (Hornberger, 1999; Gat, 2010). Both isotopes showed larger variability in those months when snow and mixed precipitation are observed, namely between November and March in more southerly CHK catchment and in April-May and November in other catchments (Fig.2a, b; Table S1). The CHK data contain samples from Tashkent, which is located on the arid plain at 486 m a.s.l. (Table 1). These account for 17% of all CHK samples. Only two samples were collected
250 in summer in Tashkent, but these two samples make the difference with other sites more pronounced (Fig. 3). Between late spring and early autumn, between-sample variability is reduced, and the standard deviations are lower except for the higher-elevation and more northerly catchments: UA and AA (Fig. 2a, b). The observed seasonal cycles are generally consistent with the previous global interpolation of precipitation isoscapes (Bowen and Revenaugh, 2003; Bowen et al., 2019) and the global high-resolution isotope precipitation data (Terzer-Wassmuth et al., 2021). However, these previous interpolated estimates
255 significantly underestimate the precipitation isotopic ratios in the study region in the cold period (Fig. 2a, b) due to the lack of data currently available in the two databases. For example, the annual mean difference between measured and derived from database (Fig. 2) varies from −0.3‰ (CHK) to 4.8‰ (CKS) for δ¹⁸O and from -6.7‰ (CHK) to 37.4 (CKS) for δD but reaches 10.1‰ (CKS) for δ¹⁸O and 52.5‰ (AA) for δD in winter (Fig.2a, b; S1).

Stepwise regression was used to determine the relationship between isotopic precipitation composition and latitude, longitude
and elevation (Table S2). The δ^{18}O and δD derived from all event-based samples collected at the individual sampling sites
located between 38.56°N – 43.04°N, 68.79°E – 76.99°E, and 486 – 3000 m a.s.l (Table 1) were the response variables. The
regression equations, derived using all available samples, were:

$$\delta^{18}O = 36.3 - 1.18Lat + 0.07Lon - 0.00001E \tag{6}$$

$$\delta D = 342 - 10.75Lat + 0.73Lon - 0.002E \tag{7}$$

where Lat is latitude (°), Lon is longitude (°), and E is elevation (m a.s.l.).

Statistically significant relationships between both δ^{18}O and δD and latitude ($p < 0.01$) were found. Relationships with
longitude and elevation were not statistically significant in the overall data set. Regression equations for meteorological
seasons are shown in Table S2. In winter, elevation was the only predictor significantly correlated with the isotopic ratios
while, in autumn, elevation and longitude were significant ($p < 0.05$). Three sites with an elevation difference of more than
800 m a.s.l. in CHK and CKS allowed examination of elevation gradients in isotopic ratios and D-excess which were calculated
using the lowest and the highest sampling points for which data were available (Table 1). For both δ^{18}O and δD, the gradients
were highest in summer but not consistent between CKS and CHK (Fig. 3). Very few samples were available for the lowest
stations and isotopic ratios at Tashkent were not consistent with the high temperatures registered at this site.

The effects of surface air temperature and precipitation depth on mean monthly values of δ^{18}O and δD were examined using
correlation analysis and the method of Dansgaard (1964). The latter suggested that a difference between isotopic ratios of δ^{18}O
averaged over warm (May-October) and cold (November-April) periods can indicate control by local temperature or
precipitation amount on isotopic ratios. Positive values of the δ^{18}O difference are typical of the high- and mid-latitude
continental stations and indicate a strong surface air temperature contribution to the precipitation isotopic composition. In the
study region, the indices were positive, ranging between 7.0‰ in CKS and 8.6‰ in UA (Table S3) demonstrating a strong
temperature effect and lesser influence of precipitation amount on isotopic ratios. Coefficients of determination for the
regression equations linking the event-based values of δD and δ^{18}O and air temperature (measured at the sampling sites) ranged
between 0.46 and 0.66 for all measurements (Equations 8-9) and for the individual sampling sites (Table S4) and were
statistically significant at the 95% confidence level - except Tashkent. The highest coefficients were obtained for the Baityk
(AA) and Oygaing (CHK) sites (0.66 and 0.64, respectively) and the lowest (0.27) for Tashkent. The δ^{18}O and δD changed by
0.62‰ and 4.68‰ per one degree temperature, respectively, for the whole data set. The highest gradients were observed at
Oygaing (0.74‰ and 5.50‰ per 1°C) and the lowest at Tashkent (0.32‰ and 2.46% per 1°C) (Table S4).

$$\delta^{18}O = 0.62t - 10.61, R^2 = 0.56 \tag{8}$$

$$\delta D = 4.68t - 71.64, R^2 = 0.54 \tag{9}$$

where t is air temperature (°C) at the sampling sites.

There was no statistically significant correlation between isotopic ratios and daily amount of precipitation in the study region.

3.2 D-excess variations over the region and elevation effects

Figure 2c shows annual cycles of D-excess. In the AA and CHK catchments, minimum D-excess values are observed in June-
July increasing in winter (AA), and spring and autumn (CHK). In UA and CKS, seasonal cycles are less pronounced (UA) or
different, with a maximum in August – September (CKS). In CKS and UA, sites are in proximity to lakes Issyk Kul (Fig. 1)
and Bolshoe Almatinskoe (BAL), respectively. The lake effect is evident in the cold season due to the contrast between an
enhanced contribution of heavier water vapour from the lake and lighter vapour delivered by the cold air masses (Bowen et

al., 2012; Xiao et al., 2017; Minder et al., 2020). This effect results in higher isotopic enrichment ratios of precipitation and lower D-excess values. In CKS, due to Issyk Kul (which does not freeze in winter in contrast to BAL), D-excess is below 10‰ between January and April.

300   D-excess values in excess of 10‰, indicate a strong contribution of recycled moisture to precipitation (Koster et al., 1993; Bershaw, 2018), and are observed in all catchments in spring (except CKS in March-April) and autumn – early winter in line with the occurrence of the wet season (Fig. 1). In the AA catchment, values more than 10‰ are observed throughout the cold season. Values more than 20‰ indicate strong re-evaporation (Fröhlich et al., 2001; Bershaw, 2018) and are evident between October and December in the AA catchment and in the individual months in the same period in CHK (October) and CKS

305   (September, December). The particularly high values reaching 29.5‰ were recorded in the AA catchment in December although this calculation is based on seven samples (Table S1).

The timing of low D-excess values, indicative of the sub-cloud evaporation effect (Fröhlich et al., 2001; Bershaw, 2018), varies between catchments (Fig. 2c; Table S1). Negative mean monthly D-excess values were observed in CHK and AA in May to September reaching –3.5‰ in July in CHK. Low precipitation amounts and higher temperatures in CHK in summer (Fig. 1)

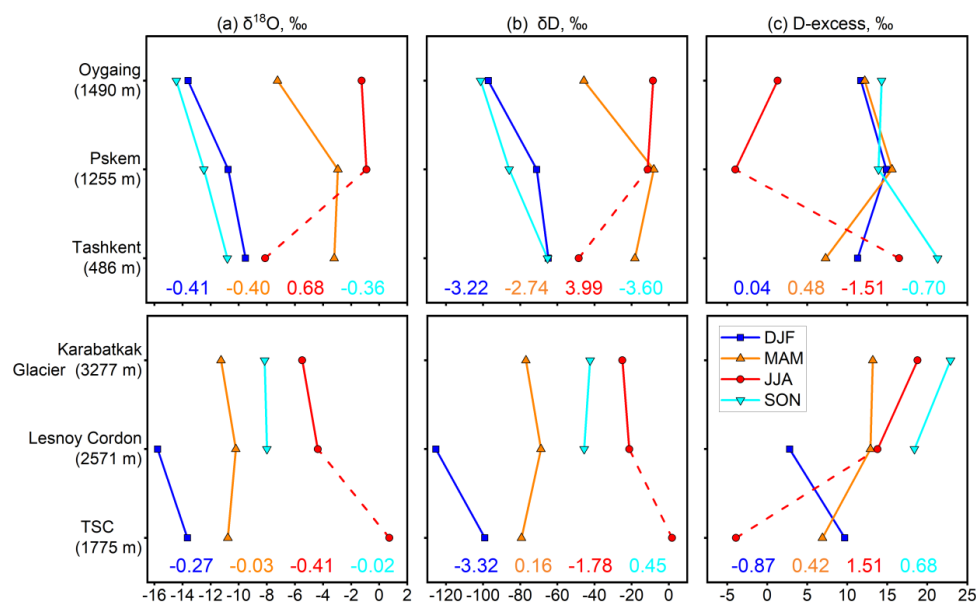310   enhance negative D-excess values and the elevational profiles of D-excess are complex (Fig. 3c).

Figure 3: Changes with elevation in (a) δ^{18}O, (b) δD, and (c) D-excess by season in CHK (upper panel) and CKS (bottom panel). Dashed lines indicate small number of samples and low precipitation per event in Tashkent and TSC. Numbers show

315   seasonal values of elevational gradients (‰ per 100 m).

The emerging patterns of changes in D-excess with elevation were inconsistent between sites and seasons (Fig. 3) partly because of the complex controls on D-excess and, potentially, because precipitation events were not always observed on the same days at different sites in the same catchment. The clearest pattern was observed in CKS in JJA where D-excess values

320   increased with altitude from –3.9‰ (n=3) at TSC located at 1755 m a.s.l. to 18.9‰ (n=28) at the Karabatkak glacier (3277 m

a.s.l.) indicating the advection of recycled moisture at higher elevations, progressive orographic moisture removal, and reduced sub-cloud evaporation typical of the mountain stations due to a smaller distance between the ground and the cloud base (Fröhlich et al., 2001; Bershaw, 2018). Similar altitudinal profiles were observed in MAM albeit with a reduced gradient (6.9‰ and 13.2‰ at TSC and Karabatkak, respectively) and in SON when data were available for the Lesnoy Cordon (2571 m a.s.l.)

325 and Karabatkak sites only (Fig. 3c). Small gradients may be attributed to the reduced sub-cloud evaporation in both spring and autumn (wet seasons) and the occurrence of predominantly liquid precipitation at lower elevations and snow at the Karabatkak glacier in spring. Thus, in CKS catchment, D-excess values for snow and rain were 9.7‰ and 15.3‰, respectively (Table S1). By contrast, in DJF, when the sub-cloud evaporation effect is absent (Fröhlich et al., 2001), D-excess values declined with elevation between the Lesnoy Cordon and TSC sites. The domination of the Siberian high limits advection of moist air to the

330 central Tien Shan in winter resulting in low precipitation across the region (Fig. 1). However, the TSC site is located in proximity to Lake Issyk Kul and it may be suggested that evaporation from the lake contributes to precipitation with less depleted isotopic signatures while the suppression of convection results in a gradient between the two sites (Fig. 3c).

In CHK, at the higher-elevation sites of Pskem (1255 m a.s.l.) and Oygaing (1490 m a.s.l.), D-excess values changed little in DJF, MAM, and SON between seasons and between the sites. The largest differences occurred at lower elevations but were

335 inconsistent between seasons. The steepest elevational gradients were observed in summer when the relationships between elevation and D-excess were non-linear and seasonal D-excess values declined from 16.5‰ (n=2) in Tashkent to a negative value of -3.9‰ (n=4) in Pskem. Similar but less pronounced gradients was observed in SON. The high D-excess values at Tashkent were not consistent with its low elevation (486 m a.s.l.), high air temperature observed during the considered precipitation events (29.8ºC) (Table S3), and low amounts of precipitation (on average, 0.1 mm per event).

340 The geographical controls over D-excess, including latitude, longitude and elevation, were investigated using stepwise regression for all the event-based samples (Table 1). The following regression equation was obtained:

$$D\text{-}excess = 51.9 - 1.29 Lat + 0.16 Lon + 0.002 E \qquad (10)$$

Longitude was significantly correlated ($p < 0.01$) with D-excess across the region and seasons. Elevation was statistically significant predictors for DFJ, JJA, MAM ($p < 0.01$) and SON ($p < 0.05$) while longitude was a significant predictor in MAM

345 ($p < 0.05$) and SON ($p < 0.05$) (Table S2).

3.3 LMWL of the mountains of Central Asia

LMWLs were calculated firstly using the whole data set and then for each catchment (Tables S5-9). The LMWL developed from the whole set of the event-based precipitation samples (Table 1; Fig. 4a) using the most common unweighted OLSR method (Section 2.3) was:

350 $$\delta D = (7.56 \pm 0.05)\delta^{18}O + (8.65 \pm 0.54), R^2 = 0.96 \qquad (11)$$

The LMWL developed from 149 mean monthly values including the Dushanbe monthly cumulative precipitation samples (Fig. 4b) using the same regression method was:

$$\delta D = (7.6 \pm 0.1)\delta^{18}O + (9.6 \pm 1.2), R^2 = 0.97 \qquad (12)$$

Figure 4 and Table S5 show the parameters of the derived regression equations. The slope and intercept values were lower

355 (Equations 11-12; Fig. 4a-c) than those of the GMWL (Dansgaard, 1964). Although, isotopic ratios are controlled by the equilibrium fractionation, in the arid regions, where significant evaporation of precipitation is observed especially during the events of light precipitation or virga, kinetic fractionation is important resulting in the difference the GMWL and LMWL slopes (Tian et al., 2007; Wang et al., 2018, 2019; Chen et al., 2021). Seasonal variations in slope and intercept values (Putman

et al., 2019), and in particular their lower values observed in summer, reflect the effects of sub-cloud evaporation too (Fig.

360   4d). For the total study area, the slope changes from 6.1±0.1 in JJA to 8.1±0.1 in DJF and intercept 2.7±0.7 in JJA to 13.8±2.1 in DJF.
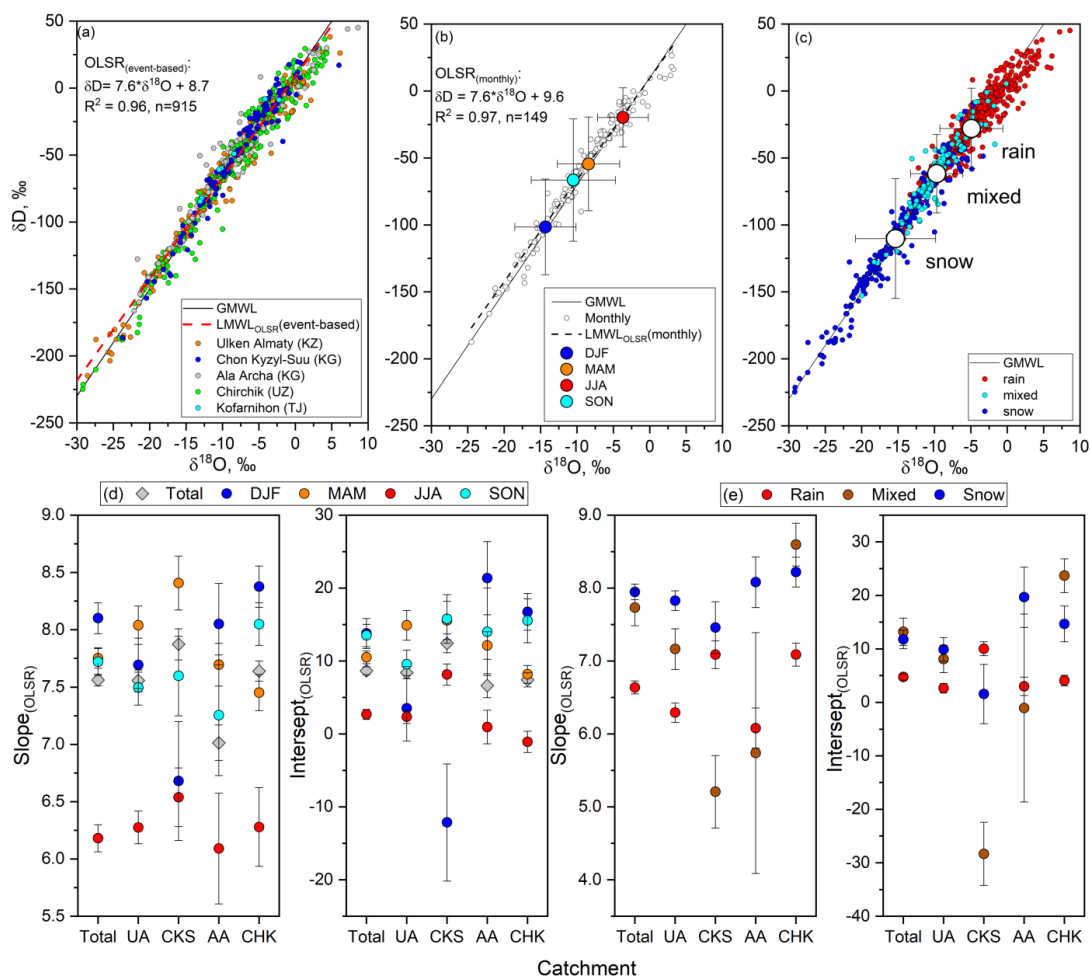

Figure 4: The upper panel shows dual δD and δ^{18}O plots for (a) the event-based samples for individual catchments, (b) monthly

365   averaged values and seasonal means, and (c) different types of precipitation. The lower panel shows the OLSR-based LMWL slopes and intercepts using (d) event-based data for each catchment by season and (e) by type of precipitation.

The effect of Lake Issyk Kul (Fig. 1a; Section 3.2) was clearly visible in the CKS data for winter. The DJF slope and intercept values in OLRS LWML, derived from 17 event-based samples, were lower than in other catchments at 6.7±0.5 and −12.1±8.3,

370   respectively (Fig. 4d). The slope value for DJF is close to that in JJA (in contrast to other catchments) indicating strong evaporation from the lake.
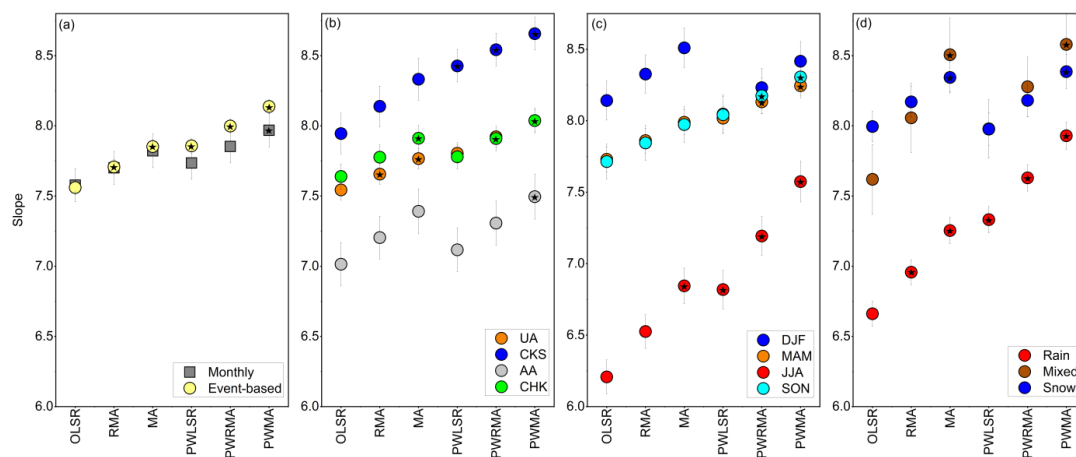
Figure 5: LMWL slopes derived from the regression equations developed using six methods (see Section 2.3 for
abbreviations) for (a) event-based and monthly data set for all samples across the region, (b) by catchment, (c) by season,
and (d) by precipitation type for the event-based samples. Statistically significant values are marked with a star sign. The
values of slopes and intercepts and the outcomes of t-test of between-method differences are presented in Tables S5-S9.

The performance of different regression methods was assessed using the RMSSEav statistics (Section 2.3). For all six methods,
RMSSEav values were close to 1 indicating good performance, however, the best regression fit was obtained by the RMA and
PWLSR methods for the non-weighted and weighted precipitation, respectively (Table S6-S9). Generally, the weighted
methods (PWLSR, PWRMA, and PWMA) generated steeper LMWL slopes than the non-weighted methods (OLSR, RMA,
and MA). However, a t-test applied to assess the differences between the regression metrics generated by the six methods and
OLSR showed that the results of the RMA method were not different from OLSR (p > 0.05) when calculations were made for
individual basins, seasons, and types of precipitation with two exceptions: (i) event-based rain only sub-sample and (ii) all
event-based samples combined across the region (Tables S5, S9). Parameters of the regression equations for each catchment,
season, and precipitation type are shown in Tables S5-S9. Here, the outcomes from the OLSR and PWLSR methods are
summarised.

For the whole region, the slopes varied from 7.6 (monthly and event-based) OLSR to 7.7 (monthly) and 7.9 (event-based)
using PWLSR (Fig. 5a). This implies that both monthly and even-based samples can be used to develop LMWL for the region.
The performance of the methods varied between catchments (Fig. 5b). The largest between-method differences were observed
in CKS (n=149) with slope values ranging between 7.9 (OLSR) and 8.4 (PWLSR). Statistically significant differences between
the non-weighted OLSR and the weighted PWLSR method were observed in AA and CHK because of the lower amounts of
precipitation, especially in CHK in summer. In the UA and CKS, the differences were not significant. The slope values
derived from the event-based precipitation data for SON (n=138) and DJF (n=168) did not vary significantly between the OLSR and
PWSLR methods (Fig. 5c) while in MAM (n=273) and JJA (n=290) they were significantly different. Larger differences were
observed in JJA (n=290) where slope values varied from 6.2 (OLSR) to 6.8 (PWLSR) (Fig. 6c). The similarly large differences
characterised the rain sample sub-set (n=514) with slope values ranging from 6.7 (OLSR) to 7.3 (PWLSR) (Fig. 5d).

## 3.4 Relationships between isotopic composition and moisture sources

Overall, 766 five-day (120 hours) back trajectories were generated for every precipitation event for four sampling points: BAL
(UA, n=338), Lesnoy Cordon (CKS, n=117), Baityk (AA, n=115), and Oygaing (CHK, n=196) (Table 1). Although the mixing

model was limited to a maximum of three contributing sources (Equations 4 - 5), the number of clusters derived for each site was not limited to three (to avoid discarding important circulation groups). Initially, the number of clusters was determined by plotting the distances between the merged clusters as a function of stage in the cluster analysis (Wilks, 1995).

405 For each site, between three and five clusters of back trajectories were identified and similar trajectory clusters from different sites were merged to form five trajectory groups (Section 2.4; Fig.6). Three criteria were used for merging the identified clusters into groups (i) direction of travel; (ii) distance travelled; (iii) whether local circulation trajectories remained within the catchment boundaries. Five synoptic groups included the northern part of Kazakhstan – southern Siberia (North - Group 1), south-eastern Europe, Black Sea and Caspian Sea (West - Group 2), Iran and eastern Mediterranean (South-West - Group 3), 410 lower reaches of the Syr Darya and Amy Darya and irrigated area around the Aral Sea (Aral - Group 4), and precipitation formed within the study catchments (Local - Group 5).

Groups 1 and 2 were identified at each site accounting for 6-26% and 5-19% of all trajectories (Table 2; Fig. 7). Group 1 trajectories were most frequent in the UA and least frequent in the CHK catchments and were the most frequent group in JJA overall (Fig. 7). Group 2 trajectories were most frequent in the CHK and least frequent in the UA and CKS catchments. Group 415 3 trajectories characterised moisture transport from Iran reaching the UA and AA catchments predominantly in DJF and MAM (Fig. 7). We note that, while limiting trajectories to 120-hour duration places their origin in Iran, the extension of their duration leads to the eastern Mediterranean albeit with higher uncertainty which increases with trajectory duration. Groups 1, 2 and 3 represented the long-distance moisture transport with the mean trajectory lengths and standard deviations 1738 ± 451, 3285 ± 1109 and 2652 ± 185 km, respectively. Trajectories from Groups 1, 2 and 3 represented moisture transport along the peripheries 420 of the low-pressure systems located north-west or west of the study region, and the differences between them were due to the latitudinal positions of the low-pressure system centres. Group 4 included shorter trajectories (1188 ± 237 km) to the UA and CKS catchments from the irrigated lands located along the Syr Darya and Amu Darya rivers and the Aral Sea. This group accounted for 33% and 44% of all trajectories to the UA and CKS catchments, respectively (Table 2; Fig. 6), with the highest frequency in MAM and JJA (Fig. 7). The lengths of the 5-day trajectories in Group 5, representing precipitation formed locally, 425 varied between 292 km at CKS to 565 km at AA catchments with a mean length of 438 ± 140 km. There is uncertainty about allocating of trajectories to Group 4 and 5 in CHK catchment because, although the Group 5 trajectories satisfied allocation criteria, the lower part of the CHK catchment is irrigated and the Chirchik is a tributary of the Amu Darya. Trajectories of this group were observed at each site accounting for 26% (UA) to 45-61% of all trajectories (Table 2).
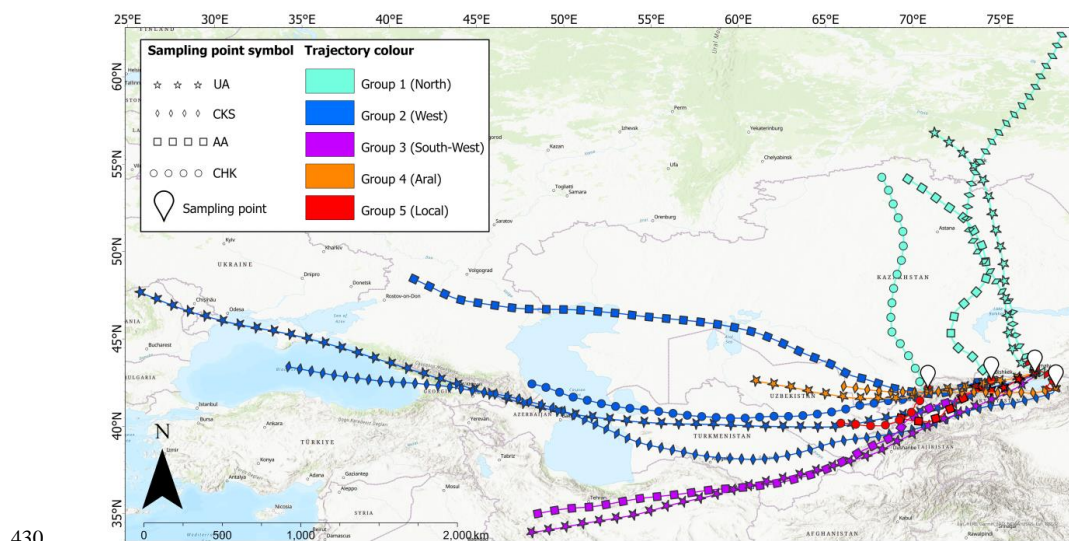
430

Figure 6: Trajectory groups including mean back trajectories (as generated by HYSPLIT) for the original clusters for four sampling sites for the study period. ESRI ArcGis Pro basemaps Word Topographic Map and World Hillshade are used as background.

435 Isotopic ratios and D-excess values averaged over the trajectory groups by site are shown in Table 2. Figures S2 and S3 further illustrate variation of seasonal values of isotopic ratios and D-excess within each original cluster by site. Statistical significance of differences between the clusters and groups (Fig. 7; S2-3) were assessed using ANOVA.

The between-group differences in δ^{18}O were largest in JJA and DJF, while in MAM and SON (wet seasons; Fig. 1c), they were not statistically significant at 95% confidence level (Fig. 7). In DJF, precipitation samples associated with Group 1 were
440 least depleted with the mean δ^{18}O value of -12.01‰ while samples associated with Group 2, representing the most long-distance transport from the west, were most depleted with mean δ^{18}O of -18.29‰ (Fig. 7a). However, the higher enrichment of δ^{18}O and δD was observed in AA for Group 2 (−6.4 ‰ and −35.0‰, respectively) where trajectories started over the East European Plain and crossed the arid west of Kazakhstan. In JJA, the highest δ^{18}O values of 0.01‰ were associated with Group 2 trajectories while the lowest mean value of -6.94‰ characterised Group 3 trajectories which also exhibited the lowest mean
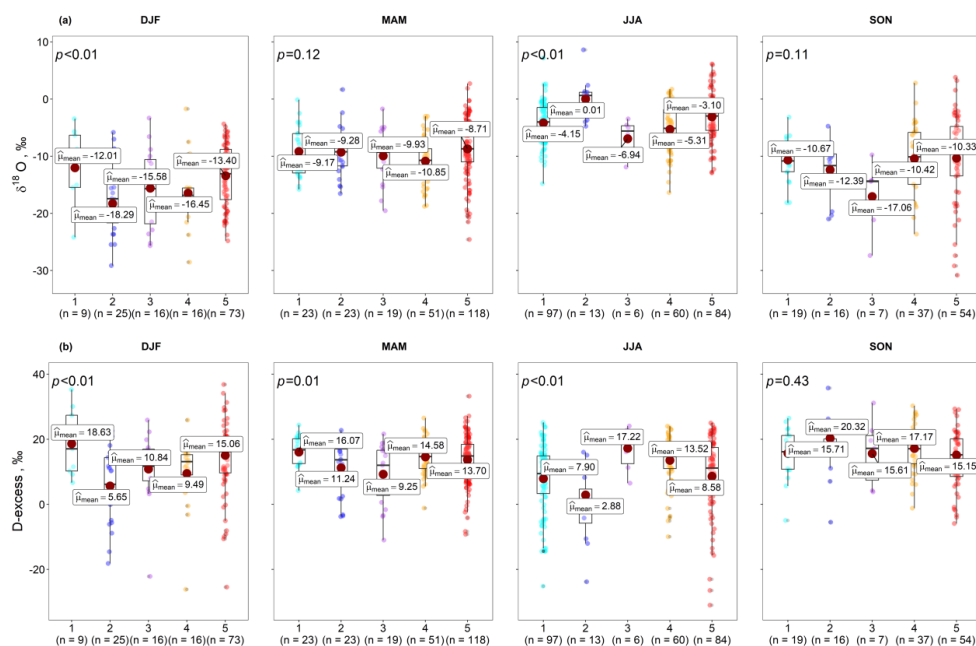445 δ^{18}O value of -17.6‰ in SON.

Figure 7: Seasonal values of of (a) δ^{18}O and (b) D-excess according to the trajectory groups. Numbers along the X-axes show the number of events in each group and season. The figure was produced using the RStudio package ggstatsplot (Patil, 2021)

450   The between-group differences in D-excess values were significantly different in all seasons except SON (Fig. 7b). In DJF, D-excess showed the opposite pattern to δ^{18}O being lowest (5.65‰) in the samples associated with Group 2 westerly trajectories and highest (18.63‰) – with Group 1 northerly trajectories (Fig. 7b). The former is associated with moisture from the Black Sea area characterized by higher relative humidity, and the latter can be associated with low relative humidity over Eurasia in winter (Bershaw, 2018; Kostrova et al., 2020). By contrast, in JJA, high humidity is observed over Siberia which

455   decreases the evaporation diffusivity ratio resulting in lower D-excess associated with Group 1 (Kostrova et al., 2020). The highest mean JJA value of 17.22‰ characterised the Group 3 trajectories arriving from Iran to the UA and AA catchments. Group 4 trajectories originating over the irrigated lands in the Aral Sea basin had the mean D-excess of 14.4‰ and 13.9‰ in the UA and CKS catchments, respectively, indicating the contribution of re-evaporated moisture to precipitation. The largest proportion of precipitation events (which were also the heaviest) was associated with the Group 5 local trajectories (n=329),

460   and precipitation formed in the local air masses upon orographic uplift (Table 2). Trajectories of this group accounted for 53% and 50% of all events in DJF and MAM. In JJA and SON, their share declined to 42% and 30% of all events, respectively, but they remained the most frequent group in SON and the second most frequent (after Group 1) in JJA. This group was characterised by the highest in-group variability in both trajectory direction, which veered strongly while the travelled distances remained short, and associated δ^{18}O and D-excess values. In the UA, AA, and CHK catchments, Group 5 trajectories arrived

465   predominantly from the south-west and corresponded to more depleted precipitation isotopic values while in CKS, they arrived from the north-east and corresponded to the higher isotopic ratios (Fig.6; Table 2). The mean D-excess values remained high in SON, DJF and MAM ranging between 13.07‰ and 15.15‰ and indicating the contribution of the re-evaporate moisture. In JJA, the mean D-excess value was 8.58‰ (which is just below the global mean) and the median value was 11.2‰ while individual D-excess values ranged between -31.0‰ and 25.0‰ (Fig. 7b). The standard deviations were high not only in JJA

470   but also in DJF at ±11.98‰ in both seasons.

Table 2: Frequency of trajectories by group and mean values (upper line) and standard deviation (lower line) of δ¹⁸O, δD and D-excess (‰) by sampling sites and trajectory clusters. C is cluster; SD is standard deviation; N is number of trajectories corresponding to individual precipitation events and their proportion of the total for each site; Lat is latitude (ºN), Lon is longitude (ºE); D is distance (km). Seasonal mean temperature and total and mean precipitation were derived for the days when precipitation samples were collected over the sampling period (Table 1) and averaged (summed) over a given trajectory cluster and season.

C	δ¹⁸O	δD	D-excess	Lat	Lon	N (%)	D	Seasonal mean t, ºC				Seasonal mean P, mm/event				Seasonal total P, mm			
	Mean (upper line) / SD (lower line)							DJF	MAM	JJA	SON	DJF	MAM	JJA	SON	DJF	MAM	JJA	SON
BAL (UA)																			
1	-6.9	-43.9	11.7	56.46	70.83	88	1625	-10.4	-2.1	7.3	-0.8	2.0	10.7	4.6	4.9	2	85	277	88
	4.4	31.2	8.6	6.41	9.27	(26)													
2	-15.9	-120.0	6.8	46.49	25.75	17	4452	-13	-6.1	10.8	2.1	4.4	5.8	2.3	6.0	35	17	5	6
	9.9	77.5	10.8	12	7.16	(5)													
3	-13.5	-98.1	10.1	33.59	48.51	31	2782	-10.2	0.0	5.6	-8	2.3	6.9	11.5	3.3	23	69	69	17
	7.1	56.0	10.8	5.93	8.78	(9)													
4	-9.8	-63.9	14.4	42.4	61.06	113	1355	-9.5	-0.2	7.3	-1.3	4.1	5.2	6.3	4.2	45	194	252	104
	6.1	46.2	6.9	5.48	6.48	(33)													
5	-8.5	-55.3	12.9	42.1	73.29	89	345	-9.6	-0.6	7.8	0.6	3.6	7.0	4.8	3.3	22	169	148	85
	6.6	48.5	10.4	2.57	6.86	(26)													
Lesnoy Cordon (CKS)																			
1	-7.7	-41.8	19.8	61.32	77.2	7	2403	-	0.6	9.1	-	-	5.2	14.1	-	-	16	56	-
	4.1	36.0	4.9	7.08	20.16	(6)													
2	-12.5	-83.8	16.2	44.68	31.4	6	3910	-4.2	-	10.4	-6.8	8.9	-	7.3	10.7	18	-	15	21
	7.7	62.0	3.5	6.33	25.5	(5)													
4	-8.1	-51.0	13.9	42.57	66.33	51	1020	-3.6	2.4	9.6	5.8	3.4	7.6	5.8	6.8	17	99	117	74
	5.5	46.7	9.1	4.71	6.68	(44)													
5	-6.3	-38.6	12.0	43.89	75.83	53	292	-	6.0	10.4	1.8	-	7.1	5.5	6.5	-	150	148	26
	4.9	37.0	10.0	3.21	3.72	(45)													
Baityk (AA)																			
1	-5.2	-31.7	9.5	53.71	70.3	14	1497	-	2.4	17.4	3.9	-	7.2	3.8	5.4	-	43	27	5
	6.1	39.8	3.5	6.55	10.14	(12)													
2	-6.4	-35.0	15.9	47.09	41.76	17	2798	-5.7	-1.2	17.6	2.6	7.4	6.2	2.9	5.2	15	12	17	36
	6.8	44.8	4.6	7.67	18.62	(15)													
3	-10.6	-70.0	14.6	34.81	48.5	17	2521	-2.9	4.9	-	-2.4	2.9	4.3	-	10.0	17	39	-	20
	4.9	36.2	1.8	7.41	7.45	(15)													
5	-9.0	-56.2	15.8	40.18	68.91	67	565	-4.7	6.0	13.6	7.4	4.0	6.6	5.3	5.1	88	132	79	51
	6.7	49.9	1.4	3.21	5.52	(58)													
Oygaing (CHK)																			
1	-4.8	-30.7	7.7	54.33	68.29	39	1427	-4.1	0.9	13.2	-	4.5	2.7	5.7	-	36	16	143	-
	5.7	42.1	12.4	6.33	8.94	(20)													
2	-11.3	-82.5	7.5	42.02	48.01	37	1981	-8.3	2.1	15.1	0.0	4.9	5.6	6.2	6.4	59	100	12	32
	7.1	55.7	10.3	8.62	10.65	(19)													
5	-9.4	-63.5	11.8	40.03	65.98	120	549	-4.1	3.0	12.8	-3.4	5.8	6.6	2.3	4.0	263	347	23	48
	7.2	57.7	10.3	3.84	6.53	(61)													

3.5 Relative contributions of moisture sources to precipitation

The cluster analysis outcomes of the HYSPLIT back trajectories combined with the isotopic signatures were used to quantify the relative contributions of the identified moisture sources to precipitation in the study region and to calculate the proportion of recycled moisture using the three-component linear mixing model (Equations 4, 5 in Section 2.5). To reconcile the number of synoptic groups with the three-component models, Groups 1, 2, and 3 were merged (westerly group) because, despite the differences in directions, they were associated with the long-distance transport along the peripheries of depressions originating over the Atlantic (Section 3.3). The three components of the mixing model (Equation 4) were: (i) δ_A – precipitation formed inland over the Aral basin (Group 4); (ii) δ_B – local moisture (Group 5); and (iii) δ_C – precipitation associated with the Atlantic depressions (Groups 1-3) and δ_P was the mean seasonal value of the isotopic ratios (Fig.8). Using the UA catchment in DJF as an example, the mean seasonal precipitation isotopic ratios (δ_P) are −134.5 ‰ for δD and − 17.9 ‰ for $\delta^{18}O$, respectively. The three components of mixing model isotopic ratios were: δ_A (−121.6 ‰ for δD and − 17.1 ‰ for $\delta^{18}O$), δ_B (−91.9 ‰ for δD and − 12.7 ‰ for $\delta^{18}O$), and δ_C (−154.3 ‰ for δD and – 19.9 ‰ for $\delta^{18}O$). In the UA, three groups of trajectories representing three moisture sources were represented in each season and in CKS in all seasons except DJF when no local trajectories were observed. Only two groups (sources) - local recycled moisture and the westerlies - were represented in the AA and CHK catchments.
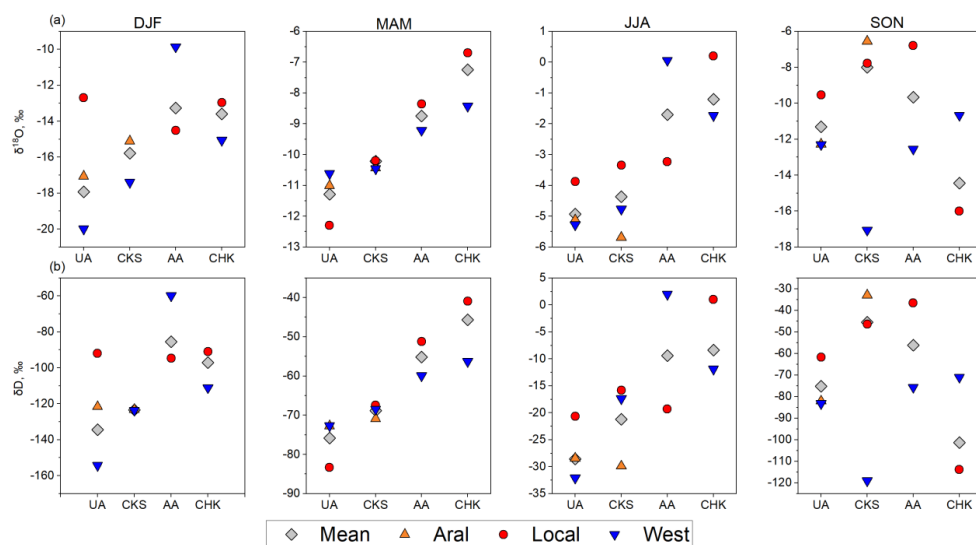
Figure 8: The values of $\delta^{18}O$ (a) and δD (b) characterising seasonal precipitation (δ_P), precipitation originating over the Aral basin (δ_A), locally formed precipitation (δ_B), and precipitation associated with the westerly transport (δ_C) for each basin.

The proportional contributions of the identified moisture sources were calculated for different catchments and seasons (Table 3). The westerly source was the main contributor to precipitation in the UA catchment in winter (54%) and in the UA and CHK in summer at 49% and 73%, respectively. The Aral basin contributed 46% in the UA in MAM, and 71.2% and 67.3% CKS in DJF and SON, respectively. In other seasons, the contribution from Aral basin varied between 29% and 37%. Contributions of the locally formed precipitation ranged from 16 to 73% and this was the dominant source in CKS, located in proximity to Lake Issyk Kul, in MAM and JJA. In AA, locally formed precipitation prevailed throughout the year and in CHK in all seasons except JJA. The predominant contribution of local sources in CHK (70%) and AA (73%) over the westerly flow

505 contribution (30% and 27%, respectively) in DJF was unexpected because to date, in climatological literature, westerly flow was seen as the main source of precipitation in winter (Lydolph, 1977). We attributed the high contribution of local sourcse to continuing evapotranspiration on the plains of Uzbekistan where temperature remain mostly positive in winter. There was uncertainty about the separation of the locally formed precipitation from that forming over the Aral basin in CHK because the catchment is a part of the Aral basin with extensive irrigation. We note that separation between sources was less clear in UA

510 in MAM and SON when precipitation maxima were observed (Fig. 1) and isotopic signatures of precipitation sourced locally and associated with the westerly transport were very similar in their isotopic composition. We also note that the absence of contribution local sources in DJF in CKS is artifact of the small number of samples collected in winter (n=7)

Table 3: Proportional contributions of moisture sources (%) to precipitation and standard errors (SE).

Catchment	Aral				Local				Westerly			
	DJF	MAM	JJA	SON	DJF	MAM	JJA	SON	DJF	MAM	JJA	SON
	Mean (upper line) / SE (lower line)											
UA	29.1	45.7	29.6	29.5	16.5	29.3	21.6	36.0	54.3	25.0	48.8	34.5
	2.0	3.1	2.1	10.7	1.0	0.6	0.6	0.4	1.0	2.7	1.7	10.4
CKS	71.2	36.5	37.0	67.3	-	54.3	51.8	21.5	28.8	9.2	11.2	11.2
	1.6	3.4	0.4	5.1		1.9	0.6	5.9	1.6	4.2	0.9	0.8
AA	-	-	-	-	73.3	54.1	53.6	50.1	26.7	45.9	46.4	49.9
					0.3	1.4	0.4	0.3	0.3	1.4	0.4	0.3
CHK	-	-	-	-	69.5	68.8	26.9	70.6	30.5	31.2	73.1	29.4
					0.5	0.4	0.4	0.6	0.5	0.4	0.4	0.6

515 4 Discussion

4.1 Filling the gap in the global database of isotopic ratios and assessing regional trends in isotopic ratios and D-excess

An important achievement of this study is the development of an extensive database of isotopic ratios of precipitation and D-excess for the mountains of CA which enabled analysis of geographical, altitudinal, and temporal patterns in isotopic composition of precipitation and attribution of precipitation to regional sources. To date, very few measurements were

520 available outside the Chinese sector of the Tien Shan. Contributing these data to GNIP (IAEA/WMO, 2015) will improve the representation of the CA mountains in the global high-resolution precipitation isoscapes database (Bowen and Revenaugh, 2003; Bowen et al., 2019; Terzer-Wassmuth et al., 2021), especially in the cold season when the differences between modelled (Bowen, 2022) and measured ratios were highest (Fig. 2). The advantages of the developed dataset are: (i) a wide geographical coverage from the northern Tien Shan (UA catchment) to the Gissar-Alay foothills (Dushanbe) (Fig. 1); (ii) sampling at

525 different elevations within two catchments because of the limited availability of such data globally (Pang et al., 2011; Natali et al, 2022); and (iii) availability of the event-based precipitation samples enabling quantification of source region contributions to CA precipitation. The measurements complied with the IAEA quality standards as confirmed by the analysis of the test samples supplied by the IAEA (Wassenaar et al., 2021) assuring the quality of the isotope measurements performed in this study.

530   The spatial variability in δ¹⁸O and δD in all seasons except autumn is characterised by an overall increase in isotopic ratios
       from north (UA), where precipitation is more depleted, to south (CHK) (Table S1). This is different from the spatial trends
       reported by Wang et al. (2016b) and Zhang and Wang (2018) for the Chinese Tien Shan where in winter, precipitation is less
       depleted in the western and northern regions and more depleted in the inner and eastern sectors while in summer, there are no
       clear spatial trends. Winter precipitation is more depleted (δ¹⁸O below –30‰) in the mountains and along the southern slope

535   of the Chinese Tien Shan (Feng et al., 2013; Wang et al., 2016b) than in our study area possibly because a number of the
       Chinese sites are located in the isotopic rain shadow while sites used in this study are located on the upwind slopes (UA, CHK)
       or near a large lake (CKS). Isotopic ratios of winter precipitation measured over the Tibetan Plateau are closer to the values
       obtained in our study area than those obtained for the Chinese Tien Shan while summer precipitation appears to be more
       depleted in Tibet where summer temperatures are lower (Liu et al., 2014; Sun et al., 2019).

540   The application of stepwise regression (Equations 6-7) showed that latitude is a statistically significant predictor of δ¹⁸O and
       δD in the overall dataset. Elevation and longitude are significant predictors in autumn and winter when westerly flow dominates
       and the data from Wang et al. (2016b) also support this conclusion. Although we used the data from all sampling sites (Table
       1), we note that the number of sampling sites was relatively small and sites in the CKS catchment were affected by Lake Issyk
       Kul. Both factors limit the performance of the regression model. For comparison, Liu et al. (2014) used 29 sampling points in

545   a similar analysis in northern China. The model can be improved in the future using isotopic data from a wider range of
       geographical locations, e.g. by combining the data sets from the CA and Chinese sectors of the Tien Shan and by including
       the newly-established sites in the western Pamir where sampling commenced in 2023.

       A clear seasonal cycle in the isotopic ratios is observed in every catchment with less depleted precipitation registered in summer
       and more depleted in winter corresponding to the annual temperature cycle (Fig. 2). This is consistent with previous global

550   studies (Bowen et al., 2019; Terzer-Wassmuth et al., 2021) and results reported for the Chinese Tien Shan (Liu et al., 2014;
       Wang et al., 2019). There was a strong positive correlation between the precipitation event-based isotopic ratios and air
       temperature with coefficients of determination of 0.46 - 0.66 (except Tashkent) similarly to the Chinese Tien Shan (Wang et
       al., 2017, 2022), northern Kazakhstan (Yapiyev et al., 2020), and other high- and mid-latitude regions (Gat and Gonfiantini,
       1981; Gat, 1996; Rozanski et al., 2013; Putman et al., 2019). The δ¹⁸O and δD changed by 0.62‰ and 4.68‰ per one degree

555   Centigrade, respectively, for the whole data set which is consistent with the results for the Upper Urumchi basin in the Chinese
       Tien Shan (Pang et al., 2011). This consistency in links between temperature and isotopic rations enables reconstruction of
       isoscapes using temperature data as a proxy. The maximum enrichment occurred between June in the south (e.g. CHK) and in
       July-August further north while the lowest isotopic ratios were registered between November and February (Fig. 2; Table S1).

       Previous studies in the Chinese Tien Shan and in the western Pamir showed that the annual cycle of D-excess was opposite to

560   those of δ¹⁸O and δD with high values in the cold season and low values in summer (Pang et al., 2011; Wang et al., 2016b;
       Zhang and Wang, 2018; Juhlke et al., 2019). In our study area, there was a clear distinction between the AA and CHK
       catchments located in the west of the study area (72-74.5ºE; Table 1) which matched the wider regional pattern, and CKS
       (78ºE) (Fig. 2c; Table S1). The annual D-excess cycle in the UA catchment in the north-east of the study area (43ºN; 77ºE)
       was less pronounced. The distinguishing characteristic of CKS is its proximity to Lake Issyk Kul which does not freeze in

565   winter. The UA sampling site was located by a much smaller (~ 0.8 km²) mountain lake which freezes in winter. While
       locations of sampling sites were to an extent defined by the practical aspects of long-term monitoring, the presence of lakes
       complicates analysis of geographical patterns of D-excess.

       The summer D-excess values in AA and CHK, calculated using unweighted precipitation, were as low as -3.5‰ and similar
       to D-excess values measured in Iran and Iraq (Juhlke et al., 2019). In CHK, low-intensity precipitation events dominated with

570   86% and 74% precipitation events producing less than 10 mm and 5 mm, respectively, in summer. At the same time, air

temperatures were high even in the middle mountains, where most samples were collected (Fig. 1; Table 1), leading to a strong sub-cloud evaporation effect. Sampling was conducted at three elevations in CHK (Fig. 3). In summer, the lowest mean D-excess value of -3.9‰ was registered at Pskem site (1255 m a.s.l.) increasing to an average of 1.3‰ at Oygaing (1490 m a.s.l.) corresponding to decreasing air temperature and the distance that rain drops travel between the cloud base and land surface

575 (Natali et al., 2022). The mean summer D-excess value of 16.5‰ in Tashkent (derived from two precipitation events only) was inconsistent with the observed meteorological conditions. We suggest that Tashkent, located in the extensively irrigated foothills and featuring urban irrigation, may exhibit higher D-excess values in summer due to the contribution of water re-evaporated from the irrigated land. Similar oasis effects were reported by Wang et al. (2016a; 2016b) and Zhang and Wang (2018), however, a larger number of samples is required to confirm this hypothesis for our study area.

580 In CKS, D-excess values fell below 10‰ between January and April increasing to 20-22‰ in August-September (Fig. 2c). Evaporation from Lake Issyk Kul continues throughout the year. During the cold season, isotopic signature of precipitation resulted from the combined effect of depleted moisture from distant sources and relatively enriched water vapour from the lake. In the warm season, when precipitation is mostly associated with local trajectories, high D-excess values resulted from strong evaporation (Bowen et al., 2012).

585 As expected, the isotopic composition of solid and mixed precipitation was highly variable at each site (Table S1) due to the fractionation effect, while rainfall was characterised by the more consistent values (Fig. 4). This variability is a source of uncertainty in modelling cold season isotopic ratios (Fig. 2) (Bowen, 2022). There was no statistically significant correlation between isotopic ratios and event precipitation depth even in the arid CHK catchment. Previous studies conducted in the neighbouring regions (Wang et al., 2018; Juhlke et al., 2019) and globally (Bowen, 2010; Bowen et al., 2019; Putman et al.,

590 2019) also concluded that this correlation was weak. Positive values of the difference between isotopic ratios of $\delta^{18}O$ averaged over warm (May-October) and cold (November-April) periods, derived from the application of Dansgaard (1964) method, were similar to those obtained by Liu et al. (2014) for northern China where seasonal variations of air temperature of approximately 30ºC were similar to the study region, and confirmed that the temperature effect dominated over that of precipitation depth.

595 **4.2. LMWL**

LMWLs were developed for the study area for the first time to complement those for the Chinese sector of the Tien Shan (Wang et al., 2018). The availability of the LMWLs is particularly important in CA because it enables quantification of the relative source contributions, including precipitation, to runoff (Bowen et al., 2018; He et al., 2019) and calculation of a lake mass balance using isotopes (Yapiyev et al., 2020). Both are relevant to adaptation policies in this water-deficient region.

600 Application of the standard OLSR method to the data from individual catchments and seasons showed that higher slope values were observed in winter and spring (7.6 – 8.4) when the air temperature is lower and relative humidity is higher, and when precipitation peaks in spring. The lowest values (6.1 – 6.3) were observed in summer suggesting strong evaporation and a contribution to precipitation from local recycled moisture (Fig. 4; Table S5). The CKS catchment featured strong seasonal variations with the lowest slope value of 6.6 in DJF, pointing at evaporation from the Issyk Kul, and the highest value of 8.4

605 in spring. The seasonal variations in LMWL slope were consistent with those in the Chinese Tien Shan (Wang et al., 2018), however it is difficult to compare spatial variations in the LMWL slopes because of a limited number of sites used in this study. A clear north to south gradient in LMWL slope is evident based on studies in the Chinese Tien Shan with the lowest values observed in the extremely arid Tarim basin (Wang et al., 2018). In our study region, the lowest summer and annual values are observed in AA rather than in CHK catchment.

610 Previous studies (Liu et al., 2014; Wang et al., 2018) demonstrated that low summer precipitation contributes to uncertainty in modelling LMWL. For this reason, three derivations of the LMWL are available for GNIP stations by using OLSR, RMA and PWLSR. Whilst there was not a statistically significant correlation between isotopic ratios and precipitation depth overall, the potential effects of low-intensity precipitation on summer isotopic ratios and in more arid regions warrantied a comparison of six different LMWL derivation methods. These covered using non-weighted and weighted precipitation and were applied

615 to the region as a whole and to the individual catchments by season (Fig. 5; Tables S6, S7). The differences in the LMWL derived from the methods using non-weighted precipitation were small and not significantly different from the OLSR although the best fit was obtained by using RMA method (Table S6-9). The difference between methods based on weighted and non-weighted precipitation were small in all seasons except summer when the largest difference between methods was observed in the AA and CHK catchments and in the rain-only sub-set (Fig. 5). The best fit was obtained using PWLSR method (Table S6-

620 9).

In the Chinese Tien Shan, similar differences between methods based on weighted and non-weighted precipitation were observed between the southern Tarim basin and the northern Junggar region (Wang et al., 2018). However, AA is in the northern part of our study area albeit in the inner Tien Shan. We, therefore, recommend that weighted precipitation and PWLSR method are used to develop LMWL during the warm season when low amounts of rainfall are observed under high

625 temperatures in CA except in catchments located in the northern outer ranges of the Tien Shan such as the UA catchment in the Ile Alatau and the Junggar region in the Chinese Tien Shan.

4.3 Main source regions of precipitation in Central Asia

In previous studies, isotopic composition of precipitation and D-excess were used to trace source regions of moisture either using the isotopic signatures directly (Bershaw, 2018) or in combination with atmospheric trajectories (Crawford et al., 2013;

630 Wang et al., 2017; Zhang and Wang, 2018; Juhlke et al., 2019). There are limitations to the former approach in CA because of its position in continental interiors away from the original marine sources of moisture, while the latter enables assessment of synoptic controls over the isotopic composition of precipitation. In this study, we used atmospheric back trajectories to examine atmospheric circulation controls using isotopic ratios and D-excess.

We experimented with trajectories of different duration finally limiting it to 120 hours to minimise uncertainty in HYSPLIT

635 modelling which increases strongly after this period of time (Draxler and Rolph, 2013). The mean water vapour residence time in the atmosphere is estimated by many studies as 8 - 10 days although its global median value was estimated as approximately five days (Van Der Ent and Tuinenburg, 2017). Therefore, limiting the length of back trajectories to 120 hours is not an issue for the shorter local and Aral Sea region trajectories. However, the identification of source regions in the westerly group (1-3) could be potentially affected especially in winter when water vapour residence time increases over the continental interiors in

640 the Northern Hemisphere compared to summer (Van Der Ent and Tuinenburg, 2017).

The westerly airflow transporting Atlantic moisture to the study region is widely acknowledged as the main source of precipitation in CA based on studies of both climate (e.g. Shahgedanova, 2002) and isotope hydrology (e.g. Tian et al., 2007; Feng et al., 2013). Our analysis showed that this pathway was detected in all seasons, however, the analysis also showed that the contribution of local recycled moisture is substantial. To quantify the relative contributions of source regions to

645 precipitation, we attempted a new approach combining the use of back trajectories with two- and three-component mixing models. One of the challenges of this approach was to reconcile the optimal number of trajectory clusters (five) with the mixing model which had a maximum of three components. We, therefore, combined three trajectory groups associated with depressions originating over the Atlantic and long-distance transport in a single group. Although groups 1 (north) and 3 (Middle East) have different isotopic signatures, they, as shown above, dominated in different seasons. Small number of

650 samples in a season or samples corresponding to some of the trajectory groups at individual sites contributed to uncertainty.

For example, there were only seven samples in CKS in winter and results for this catchments and season should be treated with caution. A wide range of isotopic signatures in SON resulted in large standard errors of the mixing model in this season especially in UA (Table 3).

The mixing model results (Table 3; Fig. 8) showed that inland recycled moisture, originating from both the vast irrigated land
655   in the Aral Sea region and from the study catchments, is the predominant source of precipitation in the study area. Precipitation maximum in all catchments occurs in MAM except UA where it peaks in May-July (Fig. 1). In this season, precipitation associated with the local trajectories accounted for 52-54% in CKS and AA increasing to 69% in CHK. The Aral Sea region contributed 46% and 37% in UA and CKS, respectively (Table 3). In UA, 30% and 22% of precipitation in JJA were associated with trajectories originating over the Aral region. The westerly group made the largest contribution in UA in JJA (49%) and
660   DJF (54%), in AA in all seasons except SON (46-50%), and in CHK in JJA (73% of what is a very low precipitation total; Fig. 1).

These results are consistent with Wang et al. (2017) who used back trajectories adjusted using specific humidity to show that the terrestrial moisture evaporated from Europe and CA may be the main source of precipitation in the Chinese Tien Shan. The results are also consistent with the outcomes of the moisture-tracking modelling studies. Tuinenburg et al. (2020) showed
665   that evaporation recycling (defined as the fraction of evaporation that precipitates in the same river basin it is evaporated from) reaches 30-40% over the Tien Shan and its foothills. The annual mean of the distance which evaporated moisture travelled in a longitudinal direction is about 2-6º (Tuinenburg et al., 2020) which is consistent with local trajectories (Table 2). Link et al. (2020) assessed the fraction of precipitation that originated as evaporation from terrestrial sources and showed that, in Kyrgyzstan, it reaches 61% making it one of the top 10 countries with the highest contributions from local, terrestrial sources.

670   We have identified a significant contribution of the local sources and the extensively irrigated lower reaches of the Amu Darya and Syr Darya as well as over 80 artificial reservoirs located in this region (Xenarios et al., 2019) to precipitation in the Tien Shan. These poses questions about the effects of both climate change including the observed and projected increase in evaporation (Ren et al., 2022; Tuinenburg et al., 2020) and water management (Wei et al., 2013) on moisture cycling in CA. Regional evapotranspiration was previously shown to provide a significant input in precipitation especially during dry periods
675   in the arid and semi-arid regions globally (Miralles et al., 2016). Water evaporated from the irrigated land contributes to precipitation over the glacierized UA and CKS catchments (and possibly CHK) contributing to snow accumulation at high elevations in MAM which is the main accumulation season in the region. This in turn, sustains seasonal snowpack and glaciers providing water for irrigation. A modelling study by de Kok et al. (2018) suggested that increased irrigation in the Tarim basin altered precipitation regime in a way that favoured glacier growth in the Kunlun Shan providing partial explanation to the
680   formation of the Karakorum-Kunlun-east Pamir anomaly (Farinotti et al., 2020). Our analysis of isotopic composition of precipitation shows that the same mechanism may operate in some regions of the Tien Shan.

5 Conclusions

The sampling programme conducted in 2019 – 2021 in the Tien Shan and its foothills produced an extensive database of isotopic ratios and D-excess filling a gap in isoscapes in the region where water cycle is highly sensitive to climate change.
685   The legacy of the programme is the installation of the Palmex Rain Samplers for the long-term collection of monthly precipitation samples for isotopic analysis in three catchments (UA, CKS, and CHK) including samplers at two elevations (700 m and 3438 m a.s.l. and away from the lake) in the UA catchment which will support further investigation in elevational gradients in isotopic ratios and D-excess. The LMWLs were developed for the region as a whole and for the individual catchments and seasons. The use of the weighted precipitation and the PWLSR method is recommended in the warm season
690   especially in the southern part of the region, while unweighted precipitation can be used in the cold season and in the outer

ranges of the northern Tien Shan using OLSR and RMA methods to derive LWWLs. The back trajectory analysis enabled the identification of the main source regions of moisture which include distant (the Black and Caspian Seas region, Iran, and northern Kazakhstan - Siberia), regional (lower reaches of the Amu Darya and Syr Darya rivers) and local (study catchments) sources. For the first time, we applied mixing model to quantify contributions of these sources to precipitation. Although the

695 model will benefit from a longer sampling period, its results were consistent with those of the moisture tracking models. An important finding was that a combined contribution of the inland re-evaporated moisture from the irrigated land in the Aral basin and local moisture recycling exceeded the contribution of the longer-distance transport associated with westerly depressions. This finding highlights strong water loss and inefficient water management in the region. It also suggests that irrigation sustained by snow and glacier melt and associated increase in evapotranspiration may benefit glacier mass balance,

700 an issue which will require further investigation. Further work to improve the spatial density of sampling sites and increase the number of samples, especially is the inner Tien Shan and the Pamir is needed to help confirm the findings.

Authors' contributions

710 MS, ZS, AW, and VY conceptualised the study; ZS processed samples and analysed the data, MS and AW supervised; ZS and MS wrote the original manuscript. Other authors participated in the sampling programme and provided meteorological data. All authors contributed to the discussion of results and the final version of the manuscript.

References

715 Aemisegger, F., Pfahl, S., Sodemann, H., Lehner, I., Seneviratne, S. I., and Wernli, H.: Deuterium excess as a proxy for continental moisture recycling and plant transpiration, Atmos. Chem. Phys., 14, 4029–4054, https://doi.org/10.5194/acp-14-4029-2014, 2014.

Aggarwal, P. K., Romatschke, U., Araguas-Araguas, L., Belachew, D., Longstaffe, F. J., Berg, P., Schumacher, C., and Funk, A.: Proportions of convective and stratiform precipitation revealed in water isotope ratios, Nat. Geosci., 9, 624–629,

720 https://doi.org/10.1038/ngeo2739, 2016.

Aizen, E. M., Aizen, V. B., Mayewski, P. A., Zhou, H., Rodda, C., Joswiak, D., Takeuchi, N., Fujita, K., Kurbatov, A., and Grigholm, B. O.: Aridity of Central Asia through the Holocene, 2017, GC41G-02, 2017.

Aizen, V., Aizen, E., Melack, J., and Martma, T.: Isotopic measurements of precipitation on central Asian glaciers (southeastern Tibet, northern Himalayas, central Tien Shan), J. Geophys. Res. Atmos., 101, 9185–9196,

725 https://doi.org/10.1029/96JD00061, 1996.

Aizen, V. B., Aizen, E. M., and Melack, J. M.: Snow distribution and melt in central Tien Shan, susamir valley, Arct. Alp.

Res., 29, 403–413, https://doi.org/10.2307/1551988, 1997.

Aizen, V. B., Aizen, E. M., Melack, J. M., Kreutz, K. J., and Cecil, L. D. W.: Association between atmospheric circulation patterns and firn-ice core records from the Inilchek glacierized area, central Tien Shan, Asia, J. Geophys. Res. D Atmos., 109, https://doi.org/10.1029/2003JD003894, 2004.

Aizen, V. B., Mayewski, P. A., Aizen, E. M., Joswiak, D. R., Surazakov, A. B., Kaspari, S., Grigholm, B., Krachler, M., Handley, M., and Finaev, A.: Stable-isotope and trace element time series from Fedchenko glacier (Pamirs) snow/firn cores, J. Glaciol., 55, 275–291, https://doi.org/10.3189/002214309788608787, 2009.

Araguás-Araguás, L., Froehlich, K., and Rozanski, K.: Deuterium and oxygen-18 isotope composition of precipitation and atmospheric moisture, Hydrol. Process., 14, 1341–1355, https://doi.org/10.1002/1099-1085(20000615)14:8<1341::AID-HYP983>3.3.CO;2-Q, 2000.

Bagheri, R., Bagheri, F., Karami, G. H., and Jafari, H.: Chemo-isotopes (18O & 2H) signatures and HYSPLIT model application: Clues to the atmospheric moisture and air mass origins, Atmos. Environ., 215, 116892, https://doi.org/10.1016/j.atmosenv.2019.116892, 2019.

Bershaw, J.: Controls on deuterium excess across Asia, Geosci., 8, https://doi.org/10.3390/geosciences8070257, 2018.

Bowen, G. J.: Isoscapes: Spatial Pattern in Isotopic Biogeochemistry, Annu. Rev. Earth Planet. Sci., 38, 161–187, https://doi.org/10.1146/annurev-earth-040809-152429, 2010.

Bowen, G. J.: The Online Isotopes in Precipitation Calculator, version OIPC3.1. http://www.waterisotopes.org, 2022.

Bowen, G. J. and Revenaugh, J.: Interpolating the isotopic composition of modern meteoric precipitation, Water Resour. Res., 39, 1–13, https://doi.org/10.1029/2003WR002086, 2003.

Bowen, G. J., Kennedy, C. D., Henne, P. D., and Zhang, T.: Footprint of recycled water subsidies downwind of Lake Michigan, 3, art53, https://doi.org/10.1890/ES12-00062.1, 2012.

Bowen, G. J., Putman, A., Brooks, J. R., Bowling, D. R., Oerter, E. J., and Good, S. P.: Inferring the source of evaporated waters using stable H and O isotopes, Oecologia, 187, 1025–1039, https://doi.org/10.1007/s00442-018-4192-5, 2018.

Bowen, G. J., Cai, Z., Fiorella, R. P., and Putman, A. L.: Isotopes in the Water Cycle: Regional- to Global-Scale Patterns and Applications, Annu. Rev. Earth Planet. Sci., 47, 453–479, https://doi.org/10.1146/annurev-earth-053018-060220, 2019.

Chen, F., Wang, S., Wu, X., Zhang, M., Argiriou, A. A., Zhou, X., and Chen, J.: Local Meteoric Water Lines in a Semi-Arid Setting of Northwest China Using Multiple Methods, 13, 2380, https://doi.org/10.3390/w13172380, 2021.

Consortium, R.: Randolph glacier inventory–a dataset of global glacier outlines: Version 6.0: technical report, global land ice measurements from space, Colorado, USA, Digit. Media. https//doi. org/10.7265, 2017.

Craig, H.: Isotopic Variations in Meteoric Waters, Science (80-.)., 133, 1702–1703, https://doi.org/10.1126/science.133.3465.1702, 1961.

Craig, H. and Gordon, L.: Deuterium and oxygen 18 variations in the ocean and the marine atmosphere, 9–130 pp., 1965.

Crawford, J., Hughes, C. E., and Parkes, S. D.: Is the isotopic composition of event based precipitation driven by moisture source or synoptic scale weather in the Sydney Basin, Australia?, J. Hydrol., 507, 213–226, https://doi.org/10.1016/j.jhydrol.2013.10.031, 2013.

Crawford, J., Hughes, C. E., and Lykoudis, S.: Alternative least squares methods for determining the meteoric water line, demonstrated using GNIP data, J. Hydrol., 519, 2331–2340, https://doi.org/10.1016/j.jhydrol.2014.10.033, 2014.

Dansgaard, W.: Stable isotopes in precipitation, Tellus A Dyn. Meteorol. Oceanogr., 16, 436,
765   https://doi.org/10.3402/tellusa.v16i4.8993, 1964.

Dorling, S. R., Davies, T. D., and Pierce, C. E.: Cluster analysis : a technique for estimating the synoptic meteorological controls on air and precipitation chemistry--results from Eskdalemuir, South Scotland, Atmos. Environ., 26, 2583–2602, 1992.

Draxler, R. R. and Rolph, G. D.: HYSPLIT (HYbrid Single-Particle Lagrangian Integrated Trajectory) Model access via
770   NOAA ARL READY Website, NOAA Air Resour. Lab. Silver Spring, MD, http://ready.arl.noaa.gov/HYSPLIT.php, 2013.

Van Der Ent, R. J. and Tuinenburg, O. A.: The residence time of water in the atmosphere revisited, Hydrol. Earth Syst. Sci., 21, 779–790, https://doi.org/10.5194/hess-21-779-2017, 2017.

Farinotti, D., Longuevergne, L., Moholdt, G., Duethmann, D., Mölg, T., Bolch, T., Vorogushyn, S., and Güntner, A.: Substantial glacier mass loss in the Tien Shan over the past 50 years, Nat. Geosci., 8, 716–722,
775   https://doi.org/10.1038/ngeo2513, 2015.

Farinotti, D., Immerzeel, W. W., de Kok, R. J., Quincey, D. J., and Dehecq, A.: Manifestations and mechanisms of the Karakoram glacier Anomaly, Nat. Geosci., 13, 8–16, https://doi.org/10.1038/s41561-019-0513-5, 2020.

Feng, F., Li, Z., Zhang, M., Jin, S., and Dong, Z.: Deuterium and oxygen 18 in precipitation and atmospheric moisture in the upper Urumqi River Basin, eastern Tianshan Mountains, Environ. Earth Sci., 68, 1199–1209,
780   https://doi.org/10.1007/s12665-012-1820-y, 2013.

Friedman, I., Machta, L., and Soller, R.: Water-vapor exchange between a water droplet and its environment, J. Geophys. Res., 67, 2761–2766, https://doi.org/10.1029/JZ067i007p02761, 1962.

Froehlich, K., Kralik, M., Papesch, W., Rank, D., Scheifinger, H., and Stichler, W.: Deuterium excess in precipitation of Alpine regions – moisture recycling, Isotopes Environ. Health Stud., 44, 61–70,
785   https://doi.org/10.1080/10256010801887208, 2008.

Fröhlich, K., Gibson, J. J., and Aggarwal, P. K.: Deuterium excess in precipitation and its climatological significance, IAEA. Study Environ. Chang. using Isot. Tech. Sci. Technol., 54–66, https://doi.org/10.1016/B978-044451669-5/50014-4, 2001.

Gat, J. R.: Oxygen and Hydrogen Isotopes in the Hydrologic Cycle, Annu. Rev. Earth Planet. Sci., 24, 225–262, https://doi.org/10.1146/annurev.earth.24.1.225, 1996.

790   Gat, J. R.: Isotope Hydrology, A Study of the Water Cycle, 189 pp., 2010.

Gat, J. R. and Gonfiantini, R.: Stable Isotope Hydrology Deuterium and Oxygen-18 in the Water Cycle. Inte, rnational At. energy agency, 339, 1981.

He, Z., Unger-shayesteh, K., Vorogushyn, S., Weise, S. M., Kalashnikova, O., Gafurov, A., Duethmann, D., Barandun, M., and Merz, B.: Constraining hydrological model parameters using water isotopic compositions in a glacierized basin , Central
795   Asia, 571, 332–348, https://doi.org/10.1016/j.jhydrol.2019.01.048, 2019.

Hoelzle, M., Barandun, M., Bolch, T., Fiddes, J., Gafurov, A., Muccione, V., Saks, T., and Shahgedanova, M.: The status and role of the alpine cryosphere in Central Asia, Aral Sea Basin Water Sustain. Dev. Cent. Asia, 2, 100–121,

https://doi.org/10.4324/9780429436475-8, 2019.

Hornberger, G. M.: Isotope Tracers in Catchment Hydrology, Eos, Trans. Am. Geophys. Union, 80, 260,
800   https://doi.org/10.1029/99EO00193, 1999.

Hughes, C. E. and Crawford, J.: A new precipitation weighted method for determining the meteoric water line for
hydrological applications demonstrated using Australian and global GNIP data, J. Hydrol., 464–465, 344–351,
https://doi.org/10.1016/j.jhydrol.2012.07.029, 2012.

IAEA/WMO: Global Network of Isotopes in Precipitation. The GNIP Database. Accessible at:
805   https://nucleus.iaea.org/wiser., 2015.

Immerzeel, W. W., Lutz, A. F., Andrade, M., Bahl, A., Biemans, H., Bolch, T., Hyde, S., Brumby, S., Davies, B. J., Elmore,
A. C., Emmer, A., Feng, M., Fernández, A., Haritashya, U., Kargel, J. S., Koppes, M., Kraaijenbrink, P. D. A., Kulkarni, A.
V., Mayewski, P. A., Nepal, S., Pacheco, P., Painter, T. H., Pellicciotti, F., Rajaram, H., Rupper, S., Sinisalo, A., Shrestha,
A. B., Viviroli, D., Wada, Y., Xiao, C., Yao, T., and Baillie, J. E. M.: Importance and vulnerability of the world's water
810   towers, Nature, 577, 364–369, https://doi.org/10.1038/s41586-019-1822-y, 2020.

Jasechko, S.: Global Isotope Hydrogeology―Review, Rev. Geophys., 57, 835–965, https://doi.org/10.1029/2018RG000627,
2019.

Jiang, J., Zhou, T., Chen, X., and Zhang, L.: Future changes in precipitation over Central Asia based on CMIP6 projections,
Environ. Res. Lett., 15, 054009, https://doi.org/10.1088/1748-9326/ab7d03, 2020.

815   Jin, L., Chen, F., Morrill, C., Otto-Bliesner, B. L., and Rosenbloom, N.: Causes of early Holocene desertification in arid
central Asia, Clim. Dyn., 38, 1577–1591, https://doi.org/10.1007/s00382-011-1086-1, 2012.

Jorba, O., Pérez, C., Rocadenbosch, F., and Baldasano, J.: Cluster Analysis of 4-Day Back Trajectories Arriving in the
Barcelona Area, Spain, from 1997 to 2002, J. Appl. Meteorol., 43, 887–901, https://doi.org/10.1175/1520-
0450(2004)043<0887:CAODBT>2.0.CO;2, 2004.

820   Juhlke, T. R., Meier, C., Van Geldern, R., Vanselow, K. A., Wernicke, J., Baidulloeva, J., Barth, J. A. C., and Weise, S. M.:
Assessing moisture sources of precipitation in the Western Pamir Mountains (Tajikistan, Central Asia) using deuterium
excess, Tellus B Chem. Phys. Meteorol., 71, 1601987, https://doi.org/10.1080/16000889.2019.1601987, 2019.

Kapitsa, V., Shahgedanova, M., Severskiy, I., Kasatkin, N., White, K., and Usmanova, Z.: Assessment of Changes in Mass
Balance of the Tuyuksu Group of Glaciers, Northern Tien Shan, Between 1958 and 2016 Using Ground-Based Observations
825   and Pléiades Satellite Imagery, Front. Earth Sci., 8, https://doi.org/10.3389/feart.2020.00259, 2020.

Kaser, G., Großhauser, M., and Marzeion, B.: Contribution potential of glaciers to water availability in different climate
regimes, Proc. Natl. Acad. Sci. U. S. A., 107, 20223–20227, https://doi.org/10.1073/pnas.1008162107, 2010.

de Kok, R. J., Tuinenburg, O. A., Bonekamp, P. N. J., and Immerzeel, W. W.: Irrigation as a Potential Driver for Anomalous
Glacier Behavior in High Mountain Asia, Geophys. Res. Lett., 45, 2047–2054, https://doi.org/10.1002/2017GL076158,
830   2018.

Koster, R. D., de Valpine, D. P., and Jouzel, J.: Continental water recycling and $H_2^{18}O$ concentrations, Geophys. Res.
Lett., 20, 2215–2218, https://doi.org/10.1029/93GL01781, 1993.

Kostrova, S. S., Meyer, H., Fernandoy, F., Werner, M., and Tarasov, P. E.: Moisture origin and stable isotope characteristics
of precipitation in southeast Siberia, Hydrol. Process., 34, 51–67, https://doi.org/10.1002/hyp.13571, 2020.

835 Kreutz, K. J., Wake, C. P., Aizen, V. B., DeWayne Cecil, L., and Synal, H. A.: Seasonal deuterium excess in a Tien Shan ice core: Influence of moisture transport and recycling in Central Asia, Geophys. Res. Lett., 30, https://doi.org/10.1029/2003GL017896, 2003.

Kutuzov, S. and Shahgedanova, M.: Glacier retreat and climatic variability in the eastern Terskey-Alatoo, inner Tien Shan between the middle of the 19th century and beginning of the 21st century, Glob. Planet. Change, 69, 59–70,
840 https://doi.org/10.1016/j.gloplacha.2009.07.001, 2009.

Lachniet, M. S. and Patterson, W. P.: Use of correlation and stepwise regression to evaluate physical controls on the stable isotope values of Panamanian rain and surface waters, J. Hydrol., 324, 115–140, https://doi.org/10.1016/j.jhydrol.2005.09.018, 2006.

Liu, J., Song, X., Yuan, G., Sun, X., and Yang, L.: Stable isotopic compositions of precipitation in China, Tellus B Chem.
845 Phys. Meteorol., 66, 22567, https://doi.org/10.3402/tellusb.v66.22567, 2014.

Lydolph, P. E.: Climates of the Soviet Union, edited by: Paul E. Lydolph and Landsberg, H. E., Elsevier Scientific Publishing Company, 443 pp., 1977.

Minder, J. R., Bartolini, W. M., Spence, C., Hedstrom, N. R., Blanken, P. D., and Lenters, J. D.: Characterizing and constraining uncertainty associated with surface and boundary layer turbulent fluxes in simulations of lake-effect snowfall,
850 Weather Forecast., 35, 467–488, https://doi.org/10.1175/WAF-D-19-0153.1, 2020.

Miralles, D. G., Nieto, R., McDowell, N. G., Dorigo, W. A., Verhoest, N. E. C., Liu, Y. Y., Teuling, A. J., Dolman, A. J., Good, S. P., and Gimeno, L.: Contribution of water-limited ecoregions to their own supply of rainfall, Environ. Res. Lett., 11, https://doi.org/10.1088/1748-9326/11/12/124007, 2016.

Natali, S., Doveri, M., Giannecchini, R., Baneschi, I., and Zanchetta, G.: Is the deuterium excess in precipitation a reliable
855 tracer of moisture sources and water resources fate in the western Mediterranean? New insights from Apuan Alps (Italy), J. Hydrol., 614, https://doi.org/10.1016/j.jhydrol.2022.128497, 2022.

Pang, Z., Kong, Y., Froehlich, K., Huang, T., Yuan, L., Li, Z., and Wang, F.: Processes affecting isotopes in precipitation of an arid region, Tellus B Chem. Phys. Meteorol., 63, 352, https://doi.org/10.1111/j.1600-0889.2011.00532.x, 2011.

Patil, I.: Visualizations with statistical details: The "ggstatsplot" approach, J. Open Source Softw., 6, 3167,
860 https://doi.org/10.21105/joss.03167, 2021.

Pérez, I. A., Artuso, F., Mahmud, M., Kulshrestha, U., Sánchez, M. L., and García, M. Á.: Applications of Air Mass Trajectories, Adv. Meteorol., 2015, 1–20, https://doi.org/10.1155/2015/284213, 2015.

Phillips, D. L. and Gregg, J. W.: Uncertainty in source partitioning using stable isotopes, Oecologia, 127, 171–179, https://doi.org/10.1007/s004420000578, 2001.

865 Putman, A. L., Fiorella, R. P., Bowen, G. J., and Cai, Z.: A Global Perspective on Local Meteoric Water Lines: Meta-analytic Insight Into Fundamental Controls and Practical Constraints, Water Resour. Res., 55, 6896–6910, https://doi.org/10.1029/2019WR025181, 2019.

Ren, Y., Yu, H., Liu, C., He, Y., Huang, J., Zhang, L., Hu, H., Zhang, Q., Chen, S., Liu, X., Zhang, M., Wei, Y., Yan, Y., Fan, W., and Zhou, J.: Attribution of Dry and Wet Climatic Changes over Central Asia, J. Clim., 35, 1399–1421,
870 https://doi.org/10.1175/JCLI-D-21-0329.1, 2022.

Rolph, G., Stein, A., and Stunder, B.: Real-time Environmental Applications and Display sYstem: READY, Environ. Model.

Softw., 95, 210–228, https://doi.org/10.1016/j.envsoft.2017.06.025, 2017.

Rozanski, K., Araguás-Araguás, L., and Gonfiantini, R.: Isotopic Patterns in Modern Global Precipitation, in: Journal of Geophysical Research Atmospheres, 1–36, https://doi.org/10.1029/GM078p0001, 2013.

875 Severskiy, I, Vilesov, E., Armstrong, R., Kokarev, A., Kogutenko, L., Usmanova, Z., Morozova, V., and Raup, B.: Changes in glaciation of the Balkhash-Alakol basin, central Asia, over recent decades, Ann. Glaciol., 57, 382–394, https://doi.org/10.3189/2016AoG71A575, 2016.

Shahgedanova, M.: In: The Physical Geography of Northern Eurasia: Russia and Neighbouring States., in: Climate at Present and in the Historical Past., Oxford University Press, 70–102, 2002.

880 Shahgedanova, M., Afzal, M., Severskiy, I., Usmanova, Z., Saidaliyeva, Z., Kapitsa, V., Kasatkin, N., and Dolgikh, S.: Changes in the mountain river discharge in the northern Tien Shan since the mid-20th Century: Results from the analysis of a homogeneous daily streamflow data set from seven catchments, J. Hydrol., 564, 1133–1152, https://doi.org/10.1016/j.jhydrol.2018.08.001, 2018.

Stein, A. F., Draxler, R. R., Rolph, G. D., StundeR, B. J. B., Cohen, M. D., and Ngan, F.: Noaa's hysplit atmospheric
885 transport and dispersion modeling system, Bull. Amer. Meteor. Soc., 96, 2059–2078, https://doi.org/https://doi.org/10.1175/BAMS-D-14-00110.1, 2015.

Sun, C., Chen, Y., Li, J., Chen, W., and Li, X.: Stable isotope variations in precipitation in the northwesternmost Tibetan Plateau related to various meteorological controlling factors, Atmos. Res., 227, 66–78, https://doi.org/10.1016/j.atmosres.2019.04.026, 2019.

890 Terzer-Wassmuth, S., Wassenaar, L. I., Welker, J. M., and Araguás-Araguás, L. J.: Improved High-Resolution Global and Regionalized Isoscapes of δ18O, δ2H, and d -Excess in Precipitation, Hydrol. Process., 35, https://doi.org/10.1002/hyp.14254, 2021.

Tian, L., Yao, T., MacClune, K., White, J. W. C., Schilla, A., Vaughn, B., Vachon, R., and Ichiyanagi, K.: Stable isotopic variations in west China: A consideration of moisture sources, J. Geophys. Res. Atmos., 112, 1–12,
895 https://doi.org/10.1029/2006JD007718, 2007.

Tuinenburg, O. A., Theeuwen, J. J. E., and Staal, A.: High-resolution global atmospheric moisture connections from evaporation to precipitation, Earth Syst. Sci. Data, 12, 3177–3188, https://doi.org/10.5194/essd-12-3177-2020, 2020.

Viviroli, D., Kummu, M., Meybeck, M., Kallio, M., and Wada, Y.: Increasing dependence of lowland populations on mountain water resources, Nat. Sustain., https://doi.org/10.1038/s41893-020-0559-9, 2020.

900 Wang, L., Dong, Y., Han, D., and Xu, Z.: Stable isotopic compositions in precipitation over wet island in Central Asia, J. Hydrol., 573, 581–591, https://doi.org/10.1016/j.jhydrol.2019.04.005, 2019.

Wang, S., Zhang, M., Che, Y., Chen, F., and Qiang, F.: Contribution of recycled moisture to precipitation in oases of arid central Asia: A stable isotope approach, Water Resour. Res., 52, 3246–3257, https://doi.org/10.1002/2015WR018135, 2016a.

905 Wang, S., Zhang, M., Hughes, C. E., Zhu, X., Dong, L., Ren, Z., and Chen, F.: Factors controlling stable isotope composition of precipitation in arid conditions: an observation network in the Tianshan Mountains, central Asia, Tellus B Chem. Phys. Meteorol., 68, 26206, https://doi.org/10.3402/tellusb.v68.26206, 2016b.

Wang, S., Zhang, M., Crawford, J., Hughes, C. E., Du, M., and Liu, X.: The effect of moisture source and synoptic

conditions on precipitation isotopes in arid central Asia, J. Geophys. Res. Atmos., 122, 2667–2682,

910   https://doi.org/10.1002/2015JD024626, 2017.

Wang, S., Zhang, M., Hughes, C. E., Crawford, J., Wang, G., Chen, F., Du, M., Qiu, X., and Zhou, S.: Meteoric water lines
in arid Central Asia using event-based and monthly data, J. Hydrol., 562, 435–445,
https://doi.org/10.1016/j.jhydrol.2018.05.034, 2018.

Wang, S., Wang, L., Zhang, M., Shi, Y., Hughes, C. E., Crawford, J., Zhou, J., and Qu, D.: Quantifying moisture recycling

915   of a leeward oasis in arid central Asia using a Bayesian isotopic mixing model, J. Hydrol., 613, 128459,
https://doi.org/10.1016/j.jhydrol.2022.128459, 2022.

Wassenaar, L., Terzer-Wassmuth, S., and Douence, C.: Progress and challenges in dual- and triple-isotope (δ18O, δ2H,
Δ17O) analyses of environmental waters: An international assessment of laboratory performance, Rapid Commun. Mass
Spectrom., 35, 1–12, https://doi.org/10.1002/rcm.9193, 2021.

920   Wei, J., Dirmeyer, P. A., Wisser, D., Bosilovich, M. G., and Mocko, D. M.: Where Does the Irrigation Water Go? An
Estimate of the Contribution of Irrigation to Precipitation Using MERRA, J. Hydrometeorol., 14, 275–289,
https://doi.org/10.1175/JHM-D-12-079.1, 2013.

Wilks: Statistical Methods in the Atmospheric Sciences, Academic Press, San Diego, 467 pp., 1995.

Wu, H., Zhang, X., Xiaoyan, L., Li, G., and Huang, Y.: Seasonal variations of deuterium and oxygen-18 isotopes and their

925   response to moisture source for precipitation events in the subtropical monsoon region, Hydrol. Process., 29, 90–102,
https://doi.org/10.1002/hyp.10132, 2015.

Xenarios, S., Schmidt-Vogt, D., Qadir, M., Janusz-Pawletta, B., and Abdullaev, I. (Eds.): The Aral Sea Basin. Water for
sustainable development in Central Asia, Routledge, 227 pp., https://doi.org/10.4324/9780429436475, 2019.

Xiao, W., Lee, X., Hu, Y., Liu, S., Wang, W., Wen, X., Werner, M., and Xie, C.: An Experimental Investigation of Kinetic

930   Fractionation of Open-Water Evaporation Over a Large Lake, J. Geophys. Res. Atmos., 122, 11,651-11,663,
https://doi.org/10.1002/2017JD026774, 2017.

Yang, X., Acharya, S., and Yao, T.: Vertical Profile of Meteoric and Surface-Water Isotopes in Nepal Himalayas to
Everest's Summit, Atmosphere (Basel)., 14, 202, https://doi.org/10.3390/atmos14020202, 2023.

Yapiyev, V., Skrzypek, G., Verhoef, A., Macdonald, D., and Sagintayev, Z.: Between boreal Siberia and arid Central Asia –

935   Stable isotope hydrology and water budget of Burabay National Nature Park ecotone (Northern Kazakhstan), J. Hydrol. Reg.
Stud., 27, 100644, https://doi.org/10.1016/j.ejrh.2019.100644, 2020.

Yoshimura, K.: Stable water isotopes in climatology, meteorology, and hydrology: A review, J. Meteorol. Soc. Japan, 93,
513–533, https://doi.org/10.2151/jmsj.2015-036, 2015.

Zhang, M. and Wang, S.: Precipitation isotopes in the Tianshan Mountains as a key to water cycle in arid central Asia, Sci.

940   Cold Arid Reg., https://doi.org/10.3724/SP.J.1226.2018.00027, 2018.